The INSR/AKT/mTOR pathway regulates the pace of myogenesis in a syndecan-3-dependent manner

Fiona K. Jones[a], Alexander Phillips[b], Andrew R. Jones[c], Addolorata Pisconti[a]

[a]Department of Biochemistry and Cell Biology, Stony Brook University, Stony Brook, NY, USA.

[b]School of Electrical Engineering, Electronics and Computer Science, University of Liverpool, Liverpool, UK

[c]Department of Biochemistry and Systems Biology, Institute of Systems, Molecular and Integrative Biology, University of Liverpool, Liverpool, UK

Correspondence to Addolorata Pisconti: *dada.pisconti@stonybrook.edu*

ABSTRACT

Muscle stem cells (MuSCs) are indispensable for muscle regeneration. A multitude of extracellular stimuli direct MuSC fate decisions from quiescent progenitors to differentiated myocytes. The activity of these signals is modulated by coreceptors such as syndecan-3 (SDC3). We investigated the global landscape of SDC3-mediated regulation of myogenesis using a phosphoproteomics approach which revealed, with the precision level of individual phosphosites, the large-scale extent of SDC3-mediated regulation of signal transduction in MuSCs. We then focused on INSR/AKT/mTOR as a key pathway regulated by SDC3 during myogenesis and mechanistically dissected SDC3-mediated inhibition of insulin receptor signaling in MuSCs. SDC3 interacts with INSR ultimately limiting signal transduction via AKT/mTOR. Both knockdown of INSR and inhibition of AKT rescue *Sdc3*$^{-/-}$ MuSC differentiation to wild type levels. Since SDC3 is rapidly downregulated at the onset of differentiation, our study suggests that SDC3 acts a timekeeper to restrain proliferating MuSC response and prevent premature differentiation.

Keywords

Muscle stem cell, AKT, insulin signaling, differentiation, mTOR, proteoglycan.

INTRODUCTION

Adult myogenesis includes both muscle growth and regeneration and is carried out by muscle stem cells (MuSCs) in response to hypertrophic stimuli or injury, respectively. MuSCs are quiescent myogenic progenitors that become activated in response to various stimuli and subsequently proliferate and differentiate inside the musculature, ultimately fusing with damaged muscle fibers (myofiber) to repair them, or with one another to generate new myofibers. During this process, MuSCs also self-regenerate, such that a pool of quiescent MuSCs poised to activate on demand is maintained, more or less, throughout life [1]. The mechanisms that regulate myogenesis and MuSC self-renewal are partly intrinsically encoded [2] and partly the result of MuSC response to environmental cues [3-9].

Syndecans, a type of transmembrane heparan sulfate proteoglycans, are multifaceted regulators of cell signaling, as their dual nature of protein and glycan confers them the ability to bind multiple partners simultaneously, thus coordinating the transduction of multiple signaling pathways [10-17]. The extent to which syndecans contribute to global signaling regulation in MuSC progeny has been recently revealed by single cell RNA-sequencing studies [18]. However, the mechanistic details underlying such powerful regulatory properties of syndecans remain poorly understood.

The four syndecans are dynamically expressed in developing [10, 19-22] and regenerating [10, 14, 19, 23-27] muscle. Based on knockout studies, syndecan-3 (SDC3) and syndecan-4 (SDC4) appear to fulfil indispensable and distinct functions in myogenesis [28, 29]. SDC3 is especially interesting in MuSC biology as its presence is necessary for maintenance of MuSC quiescence and their subsequent progression through the cell cycle once activated [26]. However, SDC3 loss is not detrimental to muscle regeneration or homeostasis, quite the contrary. *Sdc3*$^{-/-}$ mice show improved muscle maintenance and regeneration in models of acute injury, aging and muscular dystrophy [25, 26]. We and others have previously shown that this is partly due to SDC3's ability to regulate Notch and FGF signaling in a coordinated manner, which prevents MuSC exhaustion and effectively enhances regeneration [26]. However, the observation that SDC3 loss induces global changes in phospho-tyrosine levels in MuSCs [28] suggests that FGF and Notch may represent only the "tip of the iceberg" and that more signaling pathways owe their regulation to SDC3.

We used an unbiased phosphoproteomics approach to interrogate SDC3-dependent signal transduction at a global level and identified insulin signaling mediated by AKT/mTOR as a key pathway regulated by SDC3 in muscle progenitors. We then used biochemistry and cell biology approaches to dissect the insulin pathway in primary and immortalized muscle progenitors, to identify

at which level SDC3 regulates it. Lastly, we show how SDC3 expression acts as a molecular switch for the insulin/AKT/mTOR pathway promoting myoblast differentiation.

RESULTS

SDC3 depletion in myoblasts leads to increased tyrosine phosphorylation in a cell autonomous manner

Our previous work on SDC3-mediated regulation of Notch signaling strongly suggests that SDC3 loss is responsible for the cell cycle and self-renewal phenotypes observed *in vitro* and *in vivo* in a MuSC-autonomous manner [26]. To definitively test whether SDC3 functions in a cell-autonomous manner in myogenesis, we stably knocked-down SDC3 in C2C12 myoblasts (Fig. 1A) and assayed the phenotype of a stable cell line where SDC3 was heavily depleted (Fig. 1B, knockdown efficiency ≥95%) by comparison to a stable cell line transfected with an empty vector (from now on referred to as $S3^{kd}$ and Ctrl, respectively).

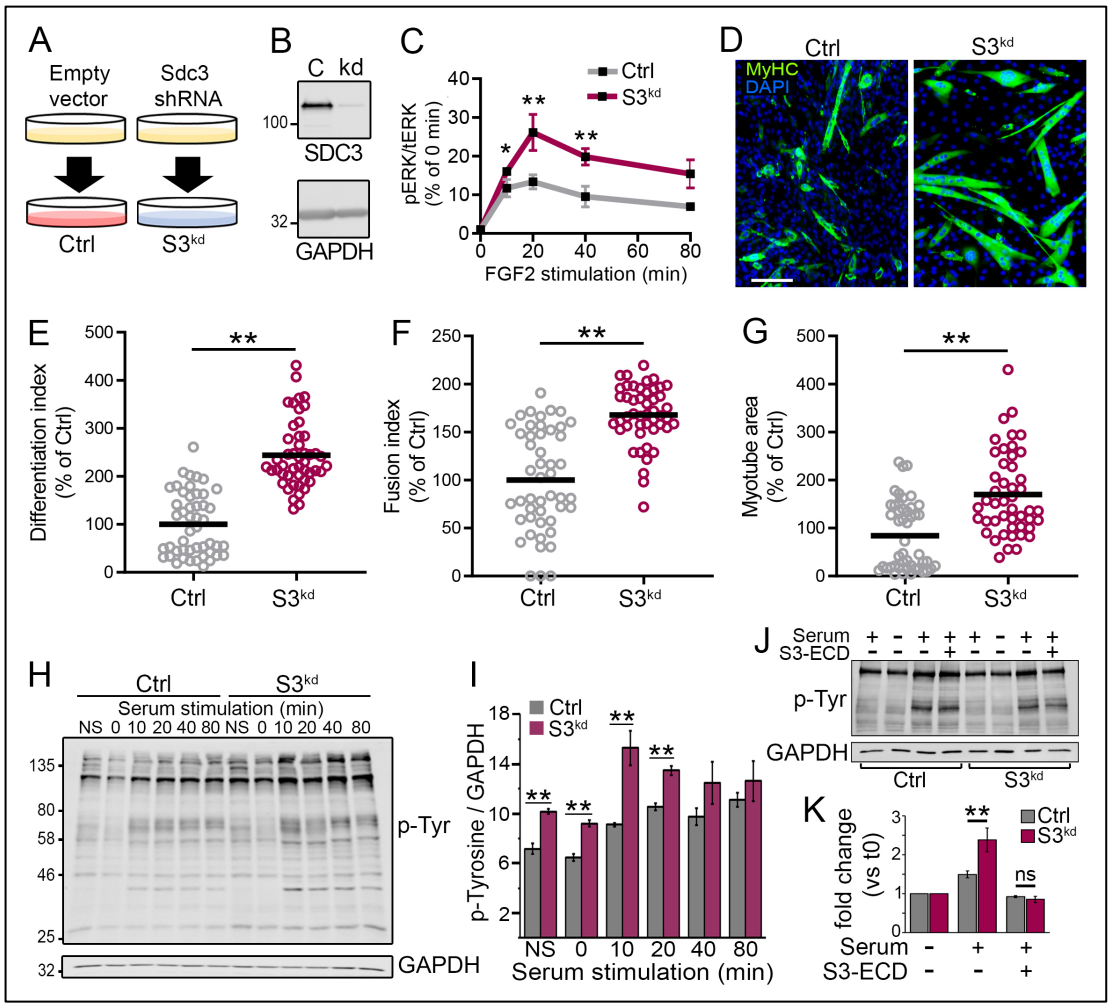

Figure 1. SDC3-depleted cells recapitulate *Sdc3*$^{-/-}$ myoblast phenotypes. (A) Schematic of the protocol used to stably knockdown SDC3 in C2C12 myoblasts. An empty vector was transfected to generate the control (Ctrl) cell line and Sdc3 shRNA was transfected to generate the SDC3-depleted (S3^{kd}) cell line. **(B)** Control **(C)** and S3^{kd} (S3) myoblasts were lysed in RIPA buffer and treated with heparinase III and chondroitinase ABC to remove glycosaminoglycans. Western blotting was used to measure the levels of SDC3 in both cell lines. GAPDH used as loading control. SDC3 is detected as a detergent-resistant dimer by western blotting. (C) Ctrl (gray) and S3^{kd} (purple) myoblasts were serum-starved for five hours then stimulated with 2 nM FGF2 over an 80 minute time-course. Cells were lysed at the indicated time points and levels of phosphorylated ERK1/2 (pERK) and total ERK1/2 (tERK) quantified via western blotting. All band intensities were quantified using ImageJ. For each of three independent experiments, pERK1/2 band intensities were normalized to total ERK1/2 band intensities at each time point and then each time point expressed as fold change of time 0. In figure, each time point subsequent to time 0 is plotted as average of the 3 experiments (N = 3). **(D)** Immunofluorescent images of Ctrl and S3^{kd} myoblasts induced to differentiate for 5 days by reducing the serum concentration. Cells were fixed then stained to detect myosin heavy chain (MyHC, green, MF20 clone antibody) and DNA (DAPI, blue) to visualize differentiated cells and nuclei respectively. Scale bar = 200 μm. N = 3. **(E-G)** Quantification of differentiation index (E), fusion index (F) and myotube area (G). Ctrl and S3^{kd} myoblasts were cultured, treated and imaged as in (D). Averages from 3 independent experiments are plotted where in each experiment data from S3^{kd} myoblasts are expressed as a percentage of Ctrl myoblasts. ** = $p < 0.01$. Each biological replicate was plated in triplicate (3 biological replicates x 3 technical replicate per cell line) and 16 images per biological replicate were scored (total N = 48 images scored per data-point). **(H)** Ctrl and S3^{kd} myoblasts were serum-starved, stimulated with 10% fetal bovine serum and then lysed at various time points over an 80 minute time course, or lysed prior to serum-starvation (NS). Cells were lysed in RIPA buffer and levels of phosphorylated tyrosines were visualized via western blotting. GAPDH was used as loading control. N = 3, representative western blot images are shown. **(I)** Quantification of (H). Error bars represent S.E.M. ** = $p < 0.01$. Averages of 3 independent experiments are plotted (N = 3). **(J)** Ctrl and S3^{kd} myoblasts were cultured and stimulated with serum as in H-I, either in the presence or absence of soluble SDC3 ectodomain (S3-ECD) then lysed and analyzed by western blotting as indicated. (K) is the quantification of (J) were the averages and S.E.M. of three independent experiments are plotted (N = 3). ** = $p < 0.01$.

SDC3 depletion in myoblasts led to a phenotype comparable to that of primary *Sdc3*$^{-/-}$ MuSC progeny [25, 26, 28], including: (i) increased responsiveness to FGF2 stimulation (Fig. 1C and Fig. S1); (ii) reduced proliferation rate (Supplementary Fig. S1); (iii) enhanced differentiation and fusion (Fig. 1D-F); and (iv) myotube hypertrophy (Fig. 1G). These findings further support the idea that loss of SDC3 affects myogenesis in a way that is largely MuSC-autonomous.

One of the most intriguing and yet unexplained phenotypes of primary *Sdc3*$^{-/-}$ MuSC progeny is an overall increase in tyrosine phosphorylation [28], which is suggestive of SDC3 playing a crucial role in the regulation of several signaling pathways simultaneously. This increased phosphotyrosine phenotype was also recapitulated in S3^{kd} myoblasts, both in serum-starved cells and, especially, in cells re-stimulated with serum (Fig. 1H-I). Since serum contains a plethora of signaling molecules (growth factors, cytokines, hormones, etc.), these data further support a role for SDC3 in the coordination of signal transduction via several receptors.

Phosphoproteomics reveals a role for SDC3 in the regulation of insulin/PI3K/mTOR signaling

Next, we sought to gain an insight into the molecular basis of the phosphotyrosine phenotype of *Sdc3*$^{-/-}$ and S3^{kd} cells, and identify candidate signaling pathways regulated by SDC3 in myoblasts. We undertook a shotgun phosphoproteomics approach and profiled phosphopeptide abundance in Ctrl and S3^{kd} myoblasts to study how they change in response to SDC3 depletion and/or serum stimulation.

Following phosphopeptide enrichment on titanium dioxide columns and label free LC-MS/MS (Fig. 2A-C and [30]) we identified and quantified changes in serine, threonine and tyrosine phosphorylation dependent on either SDC3 depletion (comparisons 1 and 2 in Fig. 2C), serum stimulation (comparisons 3 and 4 in Fig. 2C) or both combined in a two-dimensional analysis (comparison 5 in Fig. 2C). We identified a total of 11,777 peptides of which 7,190 were phosphopeptides, corresponding to 1,871 phosphoproteins (Supplementary Fig. S2). The vast majority of phosphosites identified were phosphoserine and, to a lesser extent, phosphothreonine sites, which are the most abundant in the mammalian phosphoproteome. Only a very small number of phosphotyrosine sites were identified via mass spectrometry (Supplementary Table S1) and none was differentially abundant across the conditions examined. The inability to identify a large number of phosphotyrosine sites is a well-known limitation of shotgun phosphoproteomics and is largely due to the mere scarcity of tyrosine phosphorylation compared to serine and threonine phosphorylation. However, this was not a problem for this work which did not intend to detect specific phosphotyrosine sites but rather aimed to identify candidate signaling pathways.

Firstly, we investigated the effects of SDC3 depletion on the myoblast phosphoproteome in the absence of serum (Fig. 2D, Comparison #1) and presence (Fig. 2E, Comparison #2) of serum. In both cases, the ratio between upregulated and downregulated phosphopeptides (Up/Down in Fig. 2D-E), was >1 and was greater after serum stimulation. This is consistent with our previous results on tyrosine phosphorylation (Fig. 1I), where the phospho-tyrosine complement of SDC3-depleted myoblasts was more abundant than that of Ctrl myoblasts, especially after serum stimulation. Intriguingly, SDC3 loss affected the myoblast phosphoproteome ~3 times more in the absence of serum (total Δp-peptides = 355, Fig. 2D) than in the presence of serum (Δp-peptides = 105, Fig. 2E). The latter finding suggests that SDC3 might control the extent to which a pathway is active so that when the extracellular signal that activates a given pathway is only present at low levels (e.g. the remnants of growth factors bound the extracellular and pericellular matrix after serum washout), the importance of SDC3 is more evident than when the same signal is present at saturating levels.

Secondly, we investigated myoblast response to serum stimulation in the presence (Fig. 2F, Comparison #3) and near-absence (Fig. 2G, Comparison #4) of SDC3. Both control and SDC3-depleted myoblasts showed a robust response to serum stimulation, as expected since serum contains a large number of signaling molecules. However, the overall number of phosphopeptides that changed in SDC3-depleted myoblasts (Fig. 2C and G, comparison #4 Δp-peptides = 1,416) was smaller than that in control myoblasts (Fig. 2C and F, comparison #3 Δp-peptides = 1,614), consistent with the previous

finding that in the presence of serum, SDC3 depletion leads to fewer changes to the phosphoproteome than in the absence of serum (Fig. 2D-E).

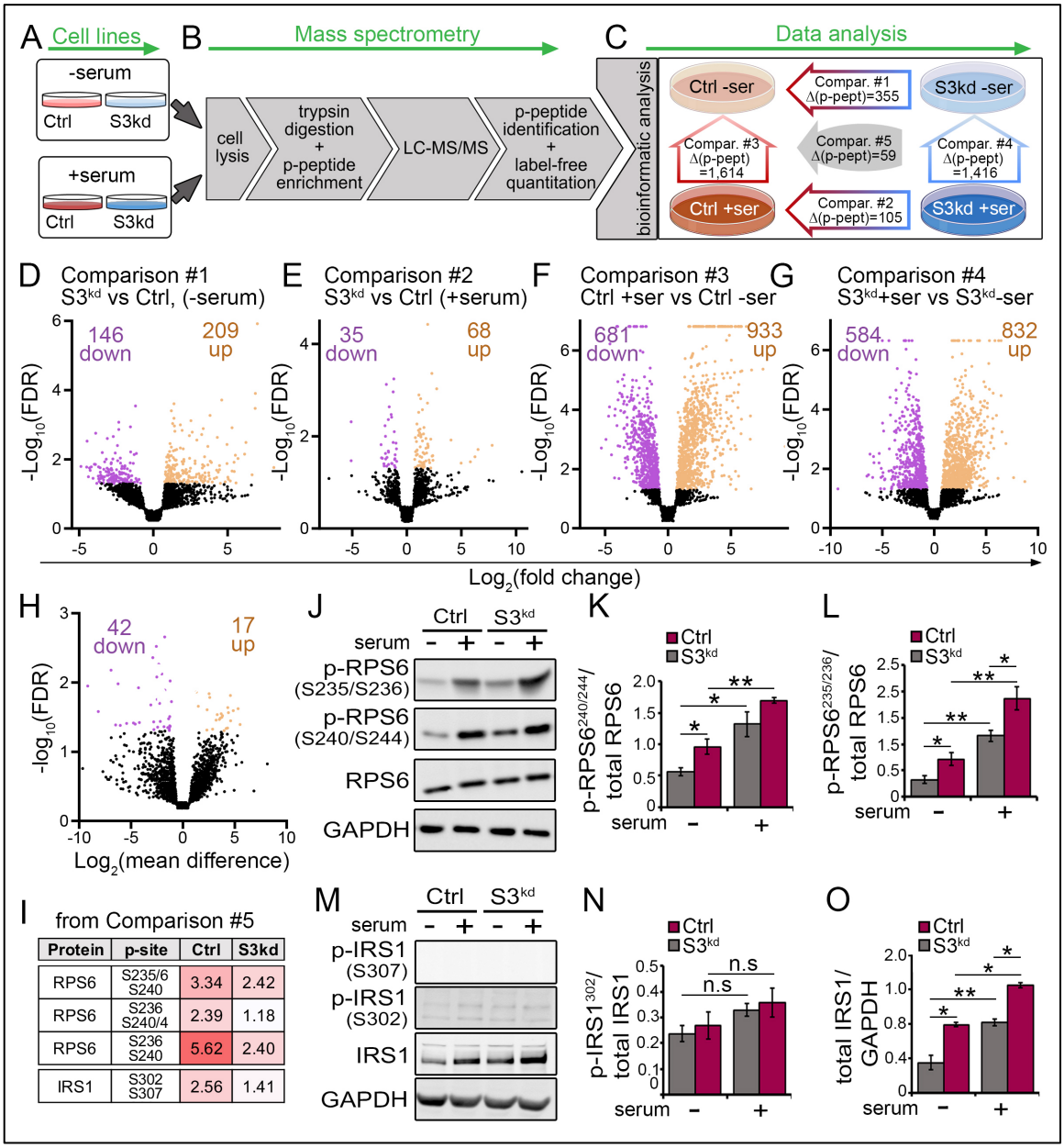

Protein	p-site	Ctrl	S3kd
RPS6	S235/6 S240	3.34	2.42
RPS6	S236 S240/4	2.39	1.18
RPS6	S236 S240	5.62	2.40
IRS1	S302 S307	2.56	1.41

Figure 2. Phosphoproteomics reveals widespread failure of S3^{kd} myoblasts to decrease signal transduction upon serum removal. (A-C) Schematic depicting the phosphoproteomics workflow. Control (Ctrl) and SDC3-depleted (S3^{kd}) myoblasts were serum-starved for 5 hours before being re-stimulated with 10% fetal bovine serum (FBS) for 10 minutes and then lysed (A). Cell lysates were enriched for phosphopeptides (p-peptide) on titanium dioxide columns and then analyzed via LC-MS/MS. P-peptides were identified and quantified using a label-free method (B). A Bayesian inference model was used to determine statistically significant differences in phosphopeptide abundance across all four datasets, which were compared pairwise in five different ways that generated five lists of differentially abundant peptides: Comparison #1 = differences between S3^{kd} and Ctrl myoblasts at the serum starved state; Comparison #2 = differences between S3^{kd} and Ctrl myoblasts at 10 minutes of serum stimulation; Comparison #3 = differences between serum-starved and serum-stimulated Ctrl myoblasts; Comparison #4 = differences between serum-starved and serum-stimulated S3^{kd} myoblasts; Comparison #5 = p-peptides regulated by both S3^{kd} depletion and serum stimulation. Δ(p-pept) = number of phosphopeptides that are significantly different in abundance between the conditions indicated by the relevant arrow (C). **(D-H)** Volcano plots displaying all phopshopeptides identified in comparisons #1-5. P-peptides were considered significant

if q-value < 0.05. N = 4 independent cell cultures per condition. **(I)** Natural log change in phosphopeptide abundance reported from phosphoproteomics data. **(J)** Control (Ctrl) and SDC3-depleted ($S3^{kd}$) myoblasts were serum-starved for 5 hours then re-stimulated with serum for 10 minutes. Cells were lysed and processed for western blotting. Levels of phosphorylated-$RPS6^{S240/S244}$, phosphorylated $RPS6^{S235/235}$ or total RPS6 were measured. GAPDH was measured as a loading control. N = 3. **(K-L)** Quantification of (H) using ImageJ. * = p<0.05, ** = p<0.01. N = 3. **(M)** The same cell lysates used for proteomics analysis shown in (A-H) were used to measure the levels of phosphorylated-$IRS1^{S307}$, $IRS1^{S302}$ and total IRS1 by western blotting. GAPDH was measured as a loading control. N = 3. **(N-O)** Quantification of (M) using ImageJ. * = p<0.05, ** = p<0.01, n.s = non-significant. N = 3.

Lastly, we carried out a two-dimensional analysis to identify phosphosites that were sensitive to both serum stimulation and SDC3 presence/absence (Fig. 2C, comparison #5 and Table S1). Not surprisingly, the number of phosphopeptides that significantly decreased as a consequence of both SDC3 depletion and serum stimulation (Fig. 2C and H, comparison #5 and Table S1, Δp-peptides DOWN = 42) was greater than the number of phosphopeptides that increased (Fig. 2C and H, comparison #5 and Table S1, Δp-peptides UP = 17).

To validate the phosphoproteomics data via a different approach, we obtained commercial antibodies that specifically recognize the phosphosites found sensitive to both serum and SDC3 (Fig. 2). Only for a few of these phosphosites could we find antibodies, including $RPS6^{S235/S236}$ and $RPS6^{S240/S244}$ (which were the top-most differentially abundant phosphopeptides sensitive to both serum and SDC3), $IRS1^{S307}$ and $IRS1^{S302}$. Western blotting analysis of phospho-RPS6 validated the phosphoproteomics data and showed that RPS6 phosphorylation both in serine 235/236 and in serine 240/244 were increased in serum-starved SDC3-depleted myoblasts compared with control myoblasts. Additionally, we validated the phosphoproteomic finding that RPS6 phosphorylation in both sites was enhanced by serum stimulation in control cells, but not in SDC3-depleted cells (Fig. 2J-L). Of the IRS1 antibodies commercially available, only the antibody directed to $IRS1^{S302}$ produced a detectable signal and showed no significant difference in response to either SDC3 depletion or serum stimulation (Fig. 2M-O). However, it is well established that IRS1 is heavily regulated at the total protein level by many of its downstream effectors including S6 kinase, which also phosphorylates RPS6 [31-33]. Indeed, we observed that total IRS1 levels followed the same trend already described for phospho-RPS6 in response to both SDC3 depletion and serum stimulation (Fig. 2M). All these observations further support the original hypothesis that SDC3 is somehow involved in repressing cell signaling in myogenesis.

SDC3 regulates insulin signaling

Once established that SDC3 is heavily involved in the regulation of the myoblast phosphoproteome, we then asked which signaling pathways are regulated by SDC3. To address this question we mapped the

proteins, and their associated phosphosites, regulated by serum stimulation in both control and SDC3-depleted myoblasts (Comparisons #3 and #4, Fig. 2C) to canonical signaling pathways using Ingenuity Pathway Analysis (IPA). Given the large number of significantly enriched pathways returned by the IPA analysis (Supplementary Table S3 and S4) and the relevance of tyrosine phosphorylation to this phosphoproteomic investigation (Fig. 1H-I) we then restricted the functional enrichment analysis to tyrosine kinase-related signalling pathways (Supplementary Table S5). Both control and SDC3-depleted myoblasts responded to serum by regulating similar signaling pathways, mostly related to growth factor and adhesion signaling (Fig. 3A). In general, it appeared that the majority of tyrosine kinase-related pathways that were significantly enriched in response to serum were more enriched in SDC3-depleted cells compared to control cells (Fig. 3A). However, nearly all of them were also less activated (smaller z-score) by serum in SDC3-depleted cells compared to control cells (Fig. 3B). The most enriched pathway in SDC3-depleted myoblasts was *Integrin signaling* (Fig. 3A). This supports our previous finding that a function of SDC3 in myoblasts and MuSCs is to regulate adhesion: primary *Sdc3*$^{-/-}$ MuSCs poorly adhere to myofibers and more easily than wild type MuSCs migrate off basal lamina-coated myofibers [25]. Consistently, we found that reduced adhesion to laminin is indeed a cell-autonomous property of myoblasts when SDC3 is depleted (Supplementary Fig. S3A). Interestingly, this adhesion defect was only statistically significant in the absence of serum and partly rescued by the addition of serum (Supplementary Fig. S3A). In contrast, adhesion of S3^{kd} myoblasts to uncoated dishes is increased both in the presence and absence of serum compared to Ctrl myoblasts (Supplementary Fig. S3B), and accompanied by increased FAK phosphorylation (Supplementary Fig. S3C-D), suggesting that a certain degree of selectivity for SDC3 exists in mediating adhesion properties of myoblasts and adhesion signaling.

Next, we interrogated the list of phosphoproteins that were differentially regulated by both SDC3 depletion and serum stimulation using the gene ontology analysis tool DAVID (Fig. 3C). Interestingly, the significantly enriched (p-value < 0.05) *Biological Processes* to which these phosphoproteins mapped, were mostly related to protein translation, with *Insulin receptor* and *mTOR signaling* appearing at the top of the list as the most enriched processes. This was consistent with *Insulin signaling* being the second most enriched signaling pathway in the response to serum (Fig. 3A) and prompted us to further investigate the role of SDC3 in the regulation of insulin and insulin receptor signaling in myogenesis.

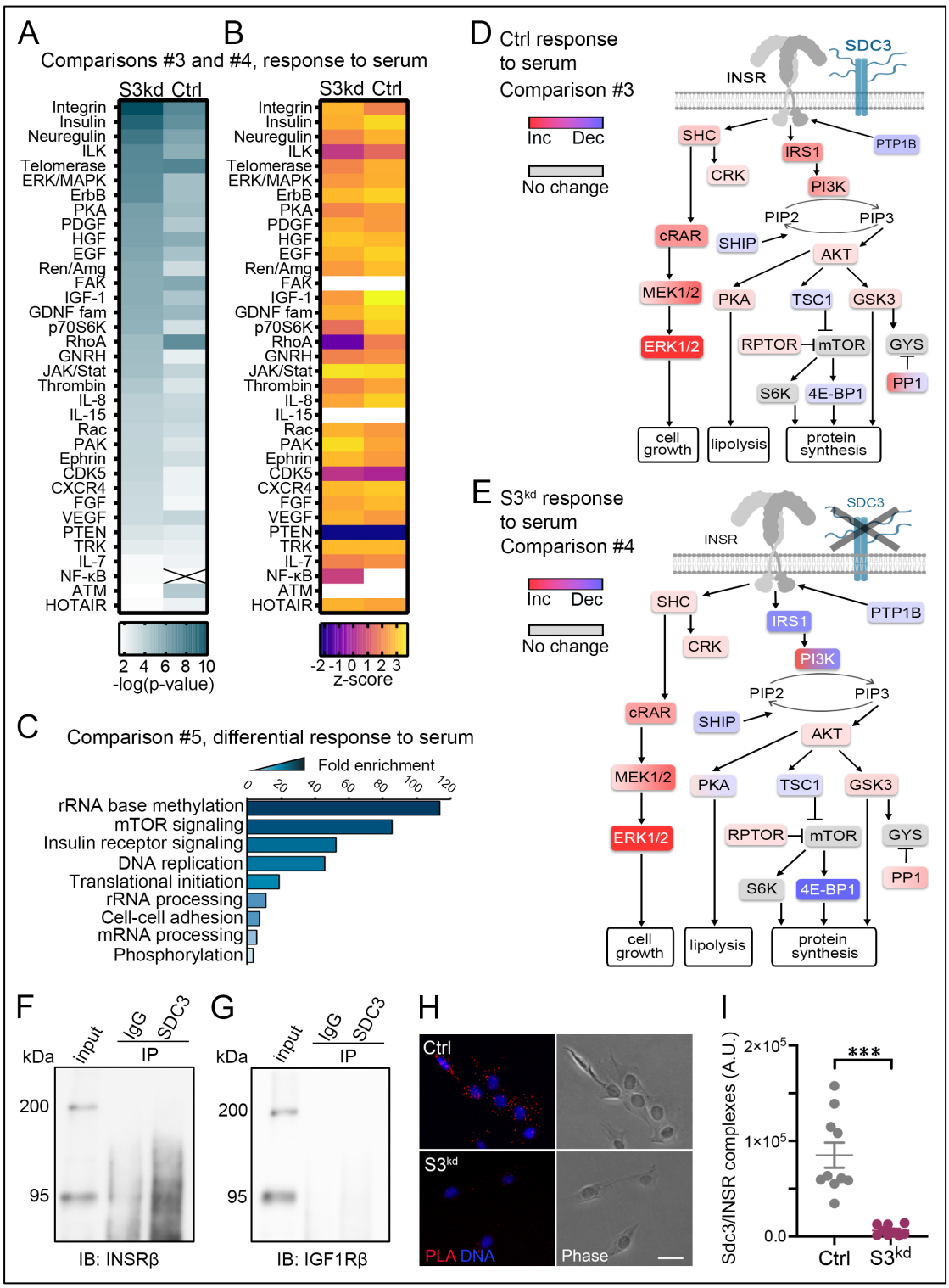

Figure 3. SDC3 coimmunoprecipitates with the insulin receptor and regulates proteins associated with insulin/AKT/mTOR signaling. (A) Phosphopeptides that were significantly up- or down-regulated when comparing the response to serum in control (Ctrl) and SDC3-depleted ($S3^{kd}$) cells, were mapped to proteins with their associated phosphosite and submitted to Ingenuity Pathway Analysis (IPA). Pathway enrichment analysis was performed, and the list of significantly enriched pathways was manually filtered to include only tyrosine kinase-related signaling pathways with a p-value < 0.05. An 'X' in the heatmap represents that the indicated pathway was not significantly enriched in the indicated cell line. Color scale: white = low enrichment, dark teal = high enrichment. **(B)** IPA's z-score for signaling pathway enrichment analysis predicts whether a pathway is activated or deactivated: a negative value indicates deactivation whereas a positive value indicates activation. Color scale for pathways that were assigned an activation score: from orange to yellow

= progressively more activated, from magenta to purple = progressively more deactivated. Where no prediction of activation level could be made the related cells are not colored. **(C)** Phosphopeptides identified as regulated by SDC3 and serum stimulation (comparison #5, Fig. 2) were mapped to their corresponding proteins and submitted to DAVID 6.8 for gene ontology analysis. Biological Processes with a $p<0.05$ were considered significant, ordered by fold enrichment and plotted. **(D-E)** The insulin receptor pathway was interrogated in IPA for further analysis. Proteins and their phosphosites were mapped by IPA and colored according to increased (red) or decreased (blue) in abundance. Where multiple phosphosites were identified, the node was colored with shades of blue and/or red. Proteins shaded in gray are essential nodes of the pathways depicted for clarity but that were not found differentially phosphorylated. **(F-G)** C2C12 myoblasts were cultured in growth medium and detached using citric saline to avoid cleaving membrane complexes. Interacting plasma membrane proteins were fixed using 2% paraformaldehyde before lysing with an immunoprecipitation-friendly buffer. SDC3 was immunoprecipitated with its interactors using a rabbit anti-SDC3 antibody, while a normal rabbit IgG was used as control. Protein complexes were then treated to remove glycosaminoglycans, subjected to western blotting and probed for either (F) the insulin receptor (INSR) or (G) the insulin-like growth factor receptor (IGF1R). The IP'ed INSR appears as a smear due to variable levels of glycosylation it harbors [41]. IB = immunoblot. IP = immunoprecipitation. N = 3. (H-I) Proximity ligation assay performed on Ctrl and $S3^{kd}$ proliferating myoblasts. Representative images from one of three independent experiments are shown in (H). Quantification of one representative of three independent experiments is quantified in (I). *** = $p < 0.001$.

Upon insulin stimulation, the insulin receptor (INSR) can signal via both the SHC/ERK pathway or via the PI3K/AKT/mTOR pathway. Although insulin signaling via ERK regulates several and diverse biological processes in various cell types, including proliferation and differentiation [34-39], in myoblasts it appears to almost exclusively promote cell growth and proliferation, while the AKT/mTOR pathway promotes a host of biological processes in myoblasts by regulating various metabolic functions, such glucose and lipid metabolism and protein translation [40]. Upon mapping to the INSR pathway the phosphoproteins that differentially responded to serum stimulation in SDC3-depleted and control myoblasts, it appeared that only the PI3K/AKT/mTOR branch of the pathway was differentially affected by the presence/absence of SDC3, while the SHC/ERK pathway was not (Fig. 3D-E).

It is well-established that the IRS1/AKT/mTOR pathway is used by both insulin and insulin-like growth factors (IGFs), whose receptor insulin-like growth factor 1 receptor (IGF1R) shares a high degree of homology with the INSR. Indeed, the INSR can be activated by IGF-1 and IGF-2, although it has greater affinity for its primary ligand insulin [42-46]. Therefore, to determine whether SDC3 selectively regulates the INSR or the IGF1R pathway, or both, we immunoprecipitated SDC3 from myoblasts and probed for both INSR and IGF1R. Despite the high homology between INSR and IGF1R, SDC3 immunoprecipitated only with the INSR but not IGF1R (Fig. 3F-G). To further test whether SDC3 and INSR are indeed in a complex, we performed a proximity ligation assay (PLA) using an antibody detecting SDC3 and one detecting INSR but not IGFR. The PLA detected more numerous, larger and brighter puncta in Ctrl cells compared to $S3^{kd}$ cells, further confirming a molecular association between SDC3 and INSR.

Our data so far strongly support a role for SDC3 in regulating signal transduction through INSR. Therefore, we decided to investigate the molecular mechanisms underlying SDC3-mediated regulation of insulin/INSR signaling.

SDC3 promotes insulin-induced proliferation but inhibits insulin-induced AKT phosphorylation in proliferating muscle progenitors.

The role of insulin signaling in myogenesis is not completely understood. It appears to promote both myoblast proliferation and differentiation [47-50]. This is intriguing since myoblast proliferation and differentiation are two mutually exclusive biological processes and it is not clear through which mechanisms the same signaling pathway is able to promote both processes.

To test the hypothesis that SDC3 regulates the INSR signaling pathway in myogenesis, we cultured control and SDC3-depleted myoblasts (Fig. 4A), as well as primary wild type and *Sdc3*$^{-/-}$ MuSC progeny (Fig. 4B), in the presence/absence of increasing concentrations of insulin. We chose to use insulin to trigger INSR activation, rather than either IGF, because insulin is INSR's primary ligand with an affinity for it ~5-fold greater than IGF2 and ~50 times greater than IGF1. After 24 hours of exposure to insulin or vehicle, control cell numbers increased in response to insulin treatment in a dose-dependent manner, while the numbers of S3^{kd} myoblasts and *Sdc3*$^{-/-}$ MuSC progeny remained constant (Fig. 4A-B), suggesting that SDC3 might be required for myoblast proliferation in response to insulin. To further test this, we measured the phosphorylation levels of AKT and ERK1/2 in control and SDC3-depleted myoblasts cultured in the presence/absence of insulin (Fig. 4C-G). Neither ERK1 nor ERK2 phosphorylation were significantly increased by chronic insulin treatment of proliferating myoblasts (Fig. 4C-E). In contrast, both control and SDC3-depleted myoblasts, cultured under proliferating conditions, responded to insulin by increasing the levels of AKT phosphorylation. However, SDC3-depleted cells, which fail to proliferate more in response to insulin, also showed greater activation of AKT in response to insulin than control cells (Fig. 4F-G). Crucially, a similar trend was observed when control and SDC3-depleted, proliferating myoblasts were serum-starved and then exposed to an acute insulin stimulation (Supplementary Fig. S4A). Thus, hyperactivation of AKT signaling in response to insulin is associated with loss of proliferative response in SDC3-depleted myoblasts and primary *Sdc3*$^{-/-}$ MuSC progeny.

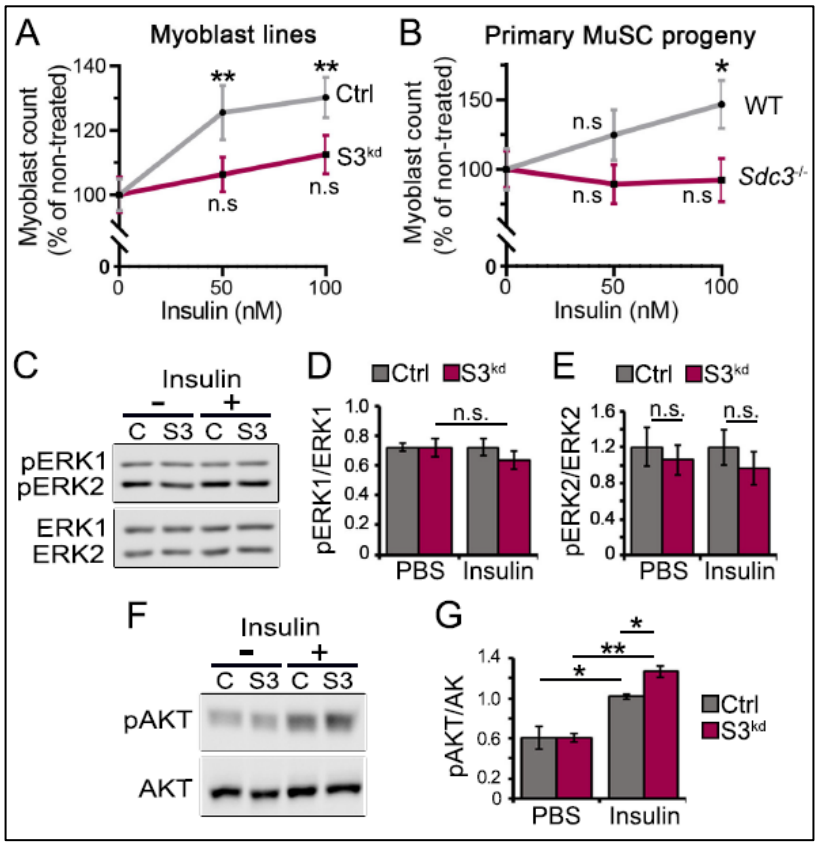

Figure 4. AKT phosphorylation induced by chronic insulin treatment is greater in proliferating S3^{kd} myoblasts compared to Ctrl myoblasts. (A) Control (Ctrl) and SDC3-depleted (S3^{kd}) cells were cultured in growth medium for 24 hours supplemented with either PBS, 50 or 100 nM insulin. Cells were stained with DAPI to visualize nuclei and the number of cells per image was counted using a bespoke Fiji script. Data are plotted as a percentage of PBS treated cells. n.s. = non-significant, ** = $p<0.01$. Averages from 3 independent experiments, are plotted. Each biological replicate was plated in triplicate (3 biological replicates x 3 technical replicates per cell line) and 30 images per biological replicate were scored (total N = 90 images per data-point). **(B)** Primary wild type (WT) and *Sdc3*$^{-/-}$ MuSC progeny were cultured and treated as in (A). Data expressed as a percentage of PBS treated cells. n.s. = non-significant * = $p<0.05$. Averages from 3 independent experiments are plotted, where 10 -15 images per biological replicate were scored (total N = minimum 30 images per data point). **(C)** Representative western blots of control (C) and SDC3-depleted (S3) myoblasts cultured in growth medium for 48 hours with either PBS or 100 nM insulin. Levels of phosphorylated-ERK1/2$^{T202/Y204}$ (pERK1, pERK2) and total ERK1/2 (ERK1, ERK2) were measured. N = 3. **(D-E)** Quantification of western blotting images as those shown in (C) using ImageJ. n.s. = non-significant. Averages from 3 independent experiments, using a total of 3 biological replicates per cell line, are plotted. N = 3. **(F)** The same cell lysates from experiments shown in (C-E) were used to measure the levels of phosphorylated in serine 473/474 (pAKT) and total AKT (AKT). Notably, AKT phosphorylation in T308/309 in proliferating Ctrl and S3^{kd} myoblasts treated with either vehicle (PBS) or insulin follows the same trend as S473/474 phosphorylation (not shown). N = 3. **(G)** Quantification of western blot images as those shown in (F). * = $p<0.05$, ** = $p<0.01$. Averages from 3 independent experiments, using a total of 3 biological replicates per cell line, are plotted. N = 3.

SDC3 loss in differentiating myoblast promotes differentiation and hyperactivation of AKT/mTOR, and impairs the response to insulin

Next, we tested the role of SDC3 in the regulation of insulin-induced myogenic differentiation in myoblast cell lines and primary MuSC progeny (Fig. 5A). In the absence of additional insulin, S3^{kd} myoblasts differentiated and fused more vigorously than Ctrl myoblasts in response to serum lowering, as previously reported [26]. Further insulin stimulation promoted differentiation and fusion in both cell lines, but Ctrl myoblasts responded to insulin to a greater extent than S3^{kd} myoblasts (Fig. 5A-C). Similar results were obtained when primary MuSC progeny isolated from wild type and *Sdc3*$^{-/-}$ mice were tested (Fig. 5D-F).

When activation of the AKT/mTOR pathway in differentiating myoblasts stimulated with insulin was assayed by measuring the levels of AKT and RPS6 phosphorylation, we observed a similar trend as shown by differentiation phenotypic markers: the absence of SDC3 led to an increase in basal

AKT/mTOR activation in differentiating myoblasts, which was accompanied by a blunted response to insulin stimulation (Fig. 5G-I). In contrast, ERK1/2 phosphorylation did not increase upon SDC3 loss in differentiating myoblasts, either under basal conditions or in response to insulin. Moreover, insulin stimulation caused a reduction in ERK1 phosphorylation in differentiating myoblasts, regardless of SDC3 expression (Fig. 5J-K). This was not surprising since a reduction in ERK1/2 signaling is known to accompany myoblast differentiation [51, 52].

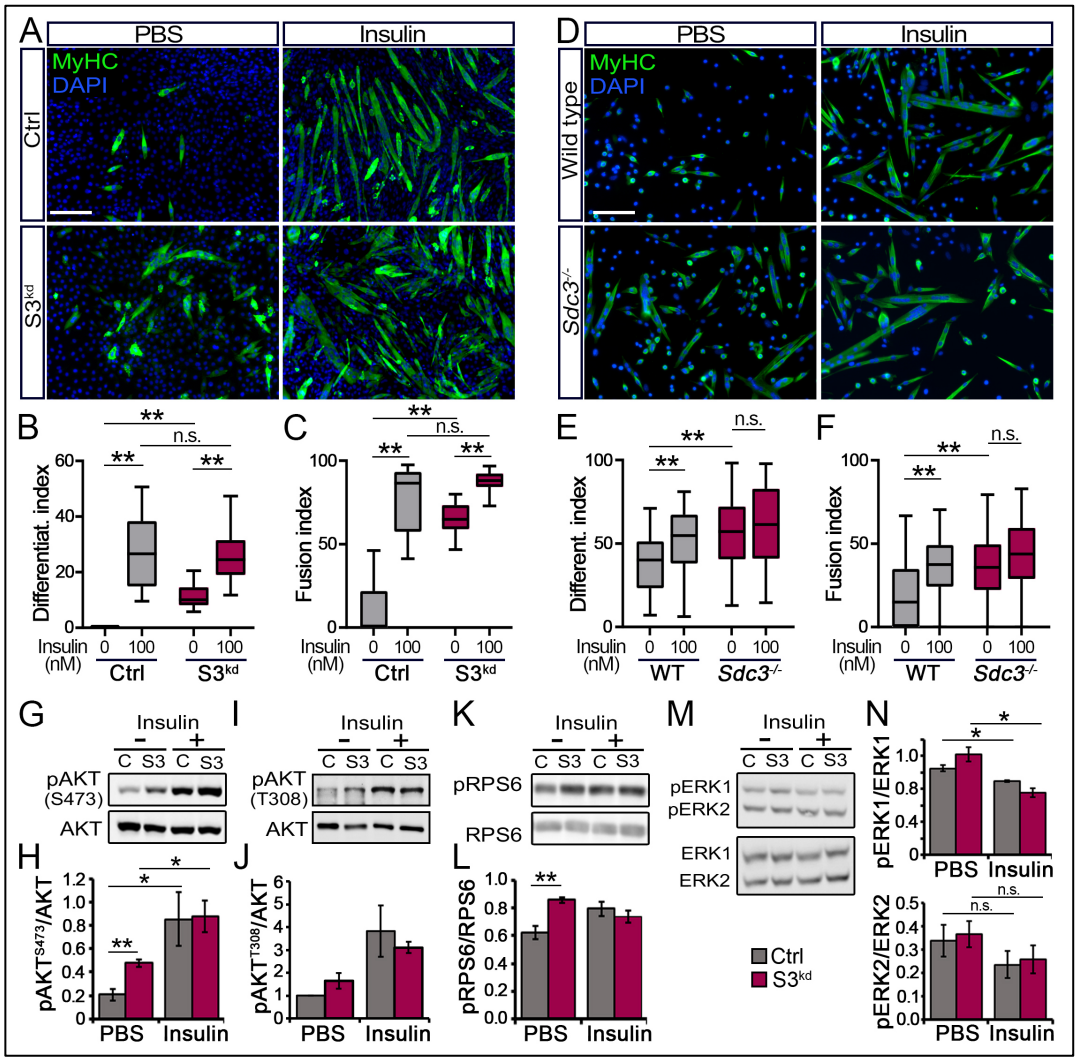

Figure 5. AKT/mTOR signaling is hyperactivated in differentiating SDC3-depleted myoblasts. (A) Representative immunofluorescent images of control (Ctrl) and SDC3-depleted ($S3^{kd}$) myoblasts induced to differentiate for 3 days by reducing the serum concentration in the presence of PBS or 100 nM insulin. Cells were stained with DAPI (blue) to visualize nuclei and an anti-myosin heavy chain (MyHC, green) antibody (MF20 clone) to detect differentiated cells. Scale bar: 200 µm. **(B-C)** Quantification of fusion and differentiation index from cells treated as in (A). n.s. = non-significant. ** = $p<0.01$. Averages from 3 independent experiments are plotted. Each biological replicate was plated in triplicate (3 biological replicates x 3 technical replicates per cell line) and 10 images per biological replicate were scored (total N = 30). **(D)** Representative immunofluorescent images of primary wild type and *Sdc3*$^{-/-}$ MuSC progeny induced to differentiate for 3 days by reducing the serum concentration in the presence of PBS or 100 nM insulin. Cells were stained with DAPI (blue) to visualize nuclei and an anti-myosin heavy chain (MyHC, green) antibody (MF20 clone) to detect differentiated cells. Scale bar: 100 µm. N = 3. **(E-F)** Quantification of fusion and differentiation index from cells treated as in (D). n.s. = non-

significant. ** = p<0.01. Averages from 3 independent experiments are plotted, where 15-20 images per biological replicate were scored (N = minimum 45 images per data point). **(G-N)** Control (C) and SDC3-depleted (S3) myoblasts were induced to differentiate for 3 days by reducing the serum concentration, in the presence of PBS or 100 nM insulin. Cells were lysed and subjected to western blotting to measure the levels of phosphorylated-AKT$^{S473/474}$ (G-H), phosphorylated-AKT$^{T308/309}$ (I-J) and total AKT (G-J); phosphorylated-RPS6$^{S240/S244}$ (pRPS6) and total RPS6 (K-L); phosphorylated-ERK1/2 and total ERK1/2 (M-N). Representative images of western blots are shown in (J), (I), (K) and (M). Quantification of western blotting images obtained from at least three independent experiments using the "Analyze Gels" function of ImageJ are plotted as averages +/- S.E.M. in (H), (J), (L) and (N). Except for pAKT$^{T308/309}$, which was only repeated on lysates from two independent experiments (hence no statistics are reported), all other western blotting analysis were repeated on lysates from 3-4 independent experiments. n.s. = non-significant, * = p<0.05, ** = p<0.01.

SDC3 inhibits the AKT/mTOR pathway in muscle progenitors thus preventing differentiation

The evidence accumulated so far suggests that, in proliferating myoblasts, SDC3 loss promotes insulin-induced activation of the AKT/mTOR pathway while inhibiting it in differentiating myoblasts. The key to understand why SDC3 loss leads to two opposite outcomes depending on the cell state is the observation that SDC3 is downregulated during myoblast differentiation (Fig. 6A) as previously reported [24] and such downregulation is accelerated in the presence of insulin (Fig. 6B). Thus, it appears that SDC3 expression acts as a molecular switch that promotes proliferation, by inhibiting AKT/mTOR, when is expressed (switch on) while allowing differentiation, by releasing the "brake" on AKT/mTOR, when is downregulated (switch off). It also appears that INSR activation, for example via insulin, exacerbates this scenario by further contributing to AKT/mTOR activation, and therefore feeding into a positive feedback loop whereby more AKT/mTOR activation leads to more differentiation and more SDC3 downregulation, which in turn leads to more AKT/mTOR activation, etc. If this hypothesis is correct, then downregulation of the INSR in differentiating *Sdc3*$^{-/-}$ muscle progeny should restore differentiation back to wild type levels. To test this hypothesis, we transfected primary wild type and *Sdc3*$^{-/-}$ MuSC progeny with siRNAs targeting the INSR (Supplementary Fig. S5A) and induced them to differentiate by serum reduction (Fig. 6C). Indeed, INSR knockdown in *Sdc3*$^{-/-}$ MuSC progeny inhibited differentiation and fusion and returned their values back to wild type levels (Fig. 6D-E and Supplementary Fig. S5B).

Even in the presence of high serum concentrations, myoblasts that have proliferated and reached confluence will spontaneously begin to differentiate, which has been described as the community effect [51, 53, 54]. We hypothesized that, upon stochastic differentiation initiation, insulin and/or IGFs contained in serum promote spontaneous progression towards terminal differentiation and fusion.

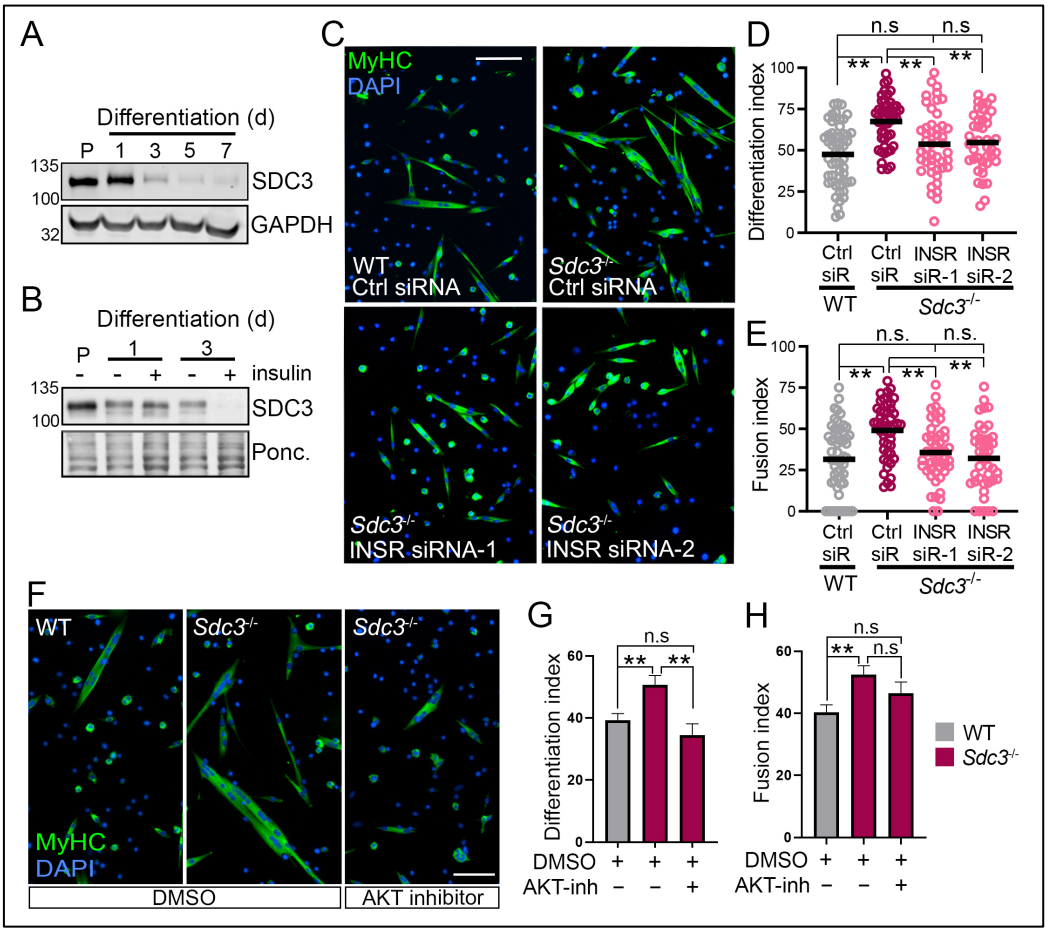

Figure 6. Knockdown of the insulin receptor and inhibition of AKT rescue the differentiation phenotype of *Sdc3*$^{-/-}$ MuSC progeny. (A) Protein levels of SDC3 in proliferating (P) and differentiating C2C12 myoblasts harvested at the indicated time points, were measured via western blotting. GAPDH was used as loading control. **(B)** Insulin treatment accelerates SDC3 downregulation during myoblast differentiation. **(C)** Immunofluorescence images of primary wild type (WT) and *Sdc3*$^{-/-}$ MuSC progeny transfected with either 10 nM scrambled siRNA (Ctrl) or insulin receptor (INSR) siRNAs, then induced to differentiate for 40 hours by reducing serum concentration. Cells were stained with DAPI (blue) to visualize nuclei and with an anti-myosin heavy chain (MyHC, green) antibody (clone MF20) to detect differentiated cells. Scale bar = 100 µm. siR = siRNA. N = 3. **(D-E)** Quantification of fusion and differentiation index from primary (WT) and *Sdc3*$^{-/-}$ MuSC progeny treated as in (B). Values from individual images were plotted as individual dots, horizontal black lines are the averages calculated across 3 biological replicates per genotype, where 15-20 images per biological replicate were scored (N = minimum 45 images per data-point). n.s. = non-significant. ** = $p<0.01$. **(F)** Immunofluorescence images of primary wild type and *Sdc3*$^{-/-}$ MuSC progeny that were cultured in growth medium for four days leading to spontaneous differentiation. Cells were treated with DMSO or 1 µM AKT inhibitor (AKT inh) from four hours after plating. Cells were stained with DAPI (blue) to visualize nuclei and an anti-myosin heavy chain (MyHC, green) antibody (MF20 clone) to detect differentiated cells. Scale bar: 100 µm. N = 3. **(G-H)** Quantification of fusion and differentiation index from (E). Error bars represent S.E.M. ** = $p< 0.01$; n.s. = non-significant. Averages from 3 (*Sdc3*$^{-/-}$ samples) and 4 (wild type samples) independent experiments are plotted, where 15-20 images per biological replicate were scored (N = minimum 45 images per data point).

This effect would then be further amplified by SDC3 downregulation (Fig. 6A) and consequent release of the SDC3-mediated brake on INSR signaling via AKT/mTOR. If this hypothesis is correct, then: (i) the pro-differentiative effect of INSR/AKT/mTOR signaling during spontaneous differentiation in high serum should be exacerbated in *Sdc3*$^{-/-}$ MuSC progeny, where AKT/mTOR is not effectively inhibited during the proliferative phase; (ii) AKT inhibition should decrease *Sdc3*$^{-/-}$ MuSC progeny spontaneous

differentiation to wild type levels. Indeed, when we cultured wild type and *Sdc3*$^{-/-}$ MuSC progeny under normal growth conditions (high serum) and allowed them to grow to confluence and then spontaneously differentiate (Fig. 6F), SDC3 loss promoted both differentiation and fusion (Fig. 6E). Furthermore, we confirmed that increased spontaneous differentiation in *Sdc3*$^{-/-}$ MuSC progeny could be rescued by AKT inhibition (Fig. 6F-G). Importantly, AKT inhibition did not significantly affect myotube fusion (Fig. 6H), suggesting that regulation of the INSR/AKT/mTOR signaling pathway affects the earlier stages of differentiation, consistent with the dynamics of SDC3 downregulation upon differentiation initiation.

DISCUSSION

We have used an unbiased phosphoproteomics approach to define the global landscape of signaling pathways regulated by SDC3 during myogenesis and identified INSR/AKT/mTOR as a key pathway regulated by SDC3 in MuSC progeny. This complements the recent finding that SDC3 regulates AKT in mesenchymal stem cells [13]. Furthermore, we show that SDC3 is in a molecular complex with the INSR but not the IGF1R, suggesting this mechanism is specific to the INSR. Following an in-depth investigation of SDC3-mediated regulation of insulin signal transduction, we discovered that SDC3 expression acts as a molecular switch allowing insulin/INSR signaling to promote proliferation when SDC3 is expressed, in the early stages of myogenesis, while promoting differentiation when SDC3 is downregulated and eventually lost, in the later stages of myogenesis.

Several signaling molecules have been shown to promote both proliferation and differentiation of MuSC progeny, including insulin and the IGFs, however this is a biological conundrum as proliferation and differentiation are two mutually exclusive processes [55-57]. Here we show that in proliferating MuSC progeny SDC3 limits AKT activation in response to insulin, which in turn prevents premature differentiation (Fig. 7A). As differentiation begins, SDC3 expression quickly decreases, releasing the inhibition on AKT and allowing differentiation to proceed (Fig. 7B).

Inhibition of premature MuSC differentiation by SDC3 during the early stages of myogenesis is an essential strategy to ensure that the MuSC progeny pool expands enough to yield the numbers of progeny necessary for a complete regeneration (Fig. 7). Indeed, as shown by us and others, SDC3 fulfils this timekeeper role also via regulation of other signaling pathways. We previously showed that SDC3 promotes MuSC progeny expansion by enhancing cleavage and activation of Notch1, which in turn inhibits differentiation and promotes cell cycle progression [26, 58]. Moreover, SDC3 is required

for Pax7 expression and maintenance of an uncommitted state [25], which is an essential mechanism in the prevention of differentiation [59, 60], and promotes MuSC adhesion to myofibers, which is required for quiescence maintenance [61].

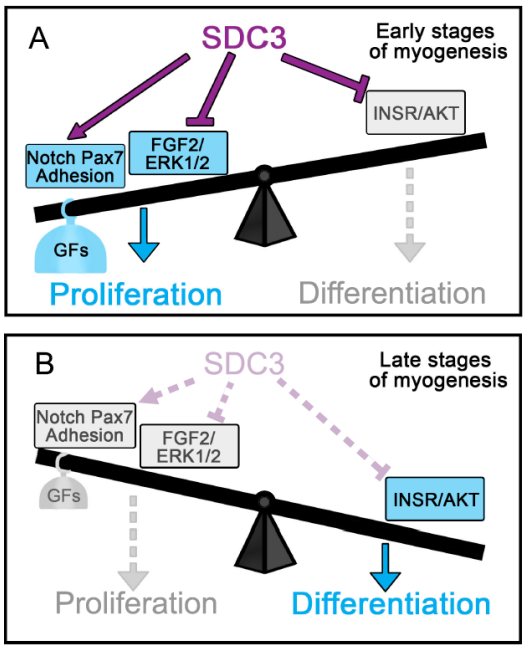

Figure 7. SDC3 is a timekeeper of myogenic differentiation. (A) During the early stages of myogenesis, SDC3 is expressed and supports proliferation by promoting Notch signaling, Pax7 expression and adhesion. At the same time SDC3 inhibits the insulin receptor (INSR)/AKT signaling pathway, which also supports proliferation by preventing premature differentiation. At this stage, growth factor (GF) signaling is also very active, further supporting proliferation, although a SDC3-mediated block on certain key GF pathways (e.g. FGF/ERK1/2 signaling pathway) poses a brake to excessive GF signaling. **(B)** During the later stages of myogenesis, SDC3 is dramatically downregulated and its ability to promote proliferation is diminished whilst differentiation via Insulin/AKT is no longer inhibited. Additionally, the reduction in growth factor signaling further tips the balance towards terminal differentiation.

An observation apparently at odds with the pro-differentiative effect of SDC3 downregulation upon differentiation initiation is that SDC3 appears to inhibit FGF2 and HGF signaling via ERK1/2 ([28] and Fig. 1C). Therefore, loss of SDC3 expression during the later stages of myogenesis should lead to ERK1/2 hyperactivation, but this would inhibit differentiation [62], while we observe enhanced differentiation when SDC3 is absent or heavily depleted. In reality, expression of ERK1/2 is also rapidly downregulated with the onset of differentiation [51], therefore positive regulation of ERK1/2 activity in the absence of SDC3 is only relevant during the early, proliferative stages of myogenesis, but not during the late, differentiative stages of myogenesis. Moreover, the overall heparan sulfate complement of MuSC progeny changes upon differentiation onset, becoming inhibitory for FGF2 signaling via ERK1/2 [63]. In fact, it is possible that SDC3-mediated inhibition of ERK1/2 in response to growth factors is the reason why regenerated myofibers are larger in *Sdc3*$^{-/-}$ mice compared to wild type controls. In the absence of SDC3, loss of proliferative capacity due to impairments in adhesion, Pax7 expression and Notch signaling and to enhanced INSR-mediated differentiation, is partly counteracted by enhanced ERK1/2 activation in response to growth factors, effectively preserving expansion of the MuSC progeny pool. Moreover, impaired Notch signaling and reduced adhesion to myofibers lead to loss of MuSC quiescence in *Sdc3*$^{-/-}$ muscles, which contributes to further expand the pool of differentiation-competent MuSC progeny, ultimately leading to generation of larger myofibers

[25, 26, 28]. In this context, it is also possible that SDC3-mediated inhibition of ERK1/2 activation by growth factors has evolved as sort of "brake" preventing excessive MuSC proliferation and eventual tumor formation [64, 65], placing SDC3 as a balancer at the center of an intricate signaling network.

An important consideration to make is the potential of compensation provided by the other three syndecans when SDC3 is depleted or ablated. We have tested whether the expression level of the other syndecans change upon SDC3 knockdown and found that mRNA levels of SDC1, SDC2 and SDC4 do not significantly change in proliferating myoblasts, but are altered in differentiated myoblasts (Supplementary Figure S6). While the other syndecans may participate in the regulation of mTOR activation and the extent and/or direction of such contribution may be altered when SDC3 is depleted or ablated, this possibility does not change the fact that: (1) we provide here strong evidence that SDC3 is closely associated with INSR, (2) SDC3 downregulation, either naturally (during the early stages of differentiation) or artificially (upon knockdown or knockout) leads to a defect on INSR signaling via AKT/mTOR. Thus, our conclusion that the expression levels of SDC3 in myoblasts determine how and how much INSR signals, remains valid, regardless of how many other receptors and co-receptors also contribute to INSR signaling via AKT/mTOR and may be altered upon SDC3 depletion or ablation.

Integrin signaling was amongst the top signaling pathways regulated by SDC3. Integrin-mediated cell adhesion may also influence insulin-mediated differentiation since integrins bind to the INSR and IRS1 upon insulin stimulation to mediate insulin signaling and promote proliferation [66]. Additionally, insulin induces dephosphorylation of focal adhesion kinase (FAK) in adherent cells and FAK/IRS1 have been shown to interact, which strongly suggests co-operation of insulin and integrin signaling [67]. Loss of SDC3 perturbs MuSC adhesion [25] and enhances differentiation. Therefore, SDC3 might regulate an insulin/integrin signaling cross-talk as syndecans cooperate with integrins to mediate cell adhesion to the ECM [15, 68]. A hypothetical model may include an integrin/INSR/SDC3 interaction in MuSC progeny that promotes proliferation in response to insulin; when SDC3 is lost this interaction is impaired and differentiation is promoted via AKT. The integrin/INSR/SDC3 complex would then prevent differentiation by inhibiting IRS1/AKT signaling, which is supported by the significant changes in the levels of total and phosphorylated IRS1 reported in this paper.

Diabetic myopathy is the reduction in muscle mass and function associated with type 1 and 2 diabetes mellitus. Skeletal muscle is heavily involved in regulating blood glucose, and in diabetic patients the total muscle mass is reduced [69]. MuSCs differentiation is impaired in diabetic mice, leading to a lack of muscle regeneration in response to injury [70]. Additionally, MuSC proliferative capacity is reduced in a rat model of metabolic syndrome, accompanied by alterations to AKT signaling and myogenic regulatory factor expression [71]. Changes in SDC3 expression have been

linked to metabolic syndrome, regulation of energy balance and obesity, all risk factors predisposing to development of type 2 diabetes mellitus [72, 73]. Moreover, fetal hyperglycemia caused by gestational diabetes of the mother causes insulin resistance in developing skeletal muscle [74]. Further work to investigate the role of SDC3/INSR/AKT signaling in a diabetic model would be advantageous to elucidate any protective effects from targeting this pathway on diabetic myopathy as well as on regulation of glucose levels.

In conclusion, our work, and that of others, establish SDC3 as an important regulator of myogenesis in charge of coordinating the delicate balance between multiple signaling pathways and biological processes. This suggests that its pharmacologic targeting might result beneficial in the context of adult muscle regeneration, developmental and obesity-related disorders.

AUTHOR CONTRIBUTIONS

Conceptualization, A.P* and F.K.J. Methodology; A.P*, F.K.J, A.J and A.P; Software, A.J and A.P; Formal Analysis, A.P*, F.K.J, A.J and A.P; Investigation, A.P* and F.K.J; Resources, A.P* and A.J; Writing – Original Draft, A.P* and F.K.J; Writing – Review & Editing, A.P*, F.K.J, A.J and A.P; Visualization, A.P* and F.K.J; Supervision, A.P* and A.J; Project Administration, A.P* and F.K.J; Funding Acquisition, A.P*. * = Addolorata Pisconti

CONFLICTS OF INTEREST

The authors declare no competing interests.

ACKNOWLEDGMENTS

The authors wish to thank the members of the Centre for Proteome Research at the University of Liverpool, especially Prof Claire Eyers and Dr Philip Brownridge. We thank Prof Dave Fernig for kindly donating recombinant FGF2 and Prof Alan Rapraeger for the rabbit anti-SDC3 antibody. A.P.* wishes to thank Niccolò P.G. Armitage for being a good baby while mummy revised and resubmitted this manuscript. This work was funded by the Biotechnology and Biological Sciences Research Council (BBSRC) in the form of DTP funding to F.K.J. and A.P.* and a Wellcome Trust ISSF fellowship to A.P.*

* = Addolorata Pisconti

Abbreviations used: MuSC, muscle stem cell; syndecan-3, SDC3; syndecan-4, SDC4, INSR, insulin receptor; IGF, insulin-like growth factor; IGF1R, insulin-like growth factor 1 receptor; S3kd, syndecan-3 knockdown; Ctrl, Control; IPA, ingenuity pathway analysis.

Keywords: Proteoglycan; Glycosaminoglycan; Cancer growth; Angiogenesis; Growth factor modulation

MATERIALS AND METHODS

A full list of reagents, tools and software used, with their unique identifiers, are available in Table S6 – Materials and Resources.

Data and Code Availability

The mass spectrometry proteomics data have been deposited to the ProteomeXchange Consortium via the PRIDE [75] partner repository with the dataset identifier PXD020123. The Bayesian Markov chain Monte Carlo (MCMC) code is available from https://github.com/PGB-LIV/JonesSDC3PhosphoproteomicsPaper. The Fiji script used to count cell nuclei and myoblast area is available from https://github.com/Piscontilab/Fiji-script

Animals

Wild type (C57Bl/6) and age and sex-matched *Sdc3*$^{-/-}$ mice [76] were housed in a pathogen-free facility at the University of Liverpool in accordance with the Animals (Scientific Procedures) Act 1986 and the EU Directive 2010/63/EU, after the local ethical review and approval by Liverpool University's Animal Welfare and Ethical Review Body.

C2C12 cell cultures

Routine culture of parental C2C12, Ctrl and S3^{kd} myoblasts was performed under humidified atmosphere of 5% CO_2 and atmospheric O_2 at 37 °C. Growth medium was composed of DMEM (D6429 Sigma-Aldrich), 10% foetal bovine serum (Gibco), 1% penicillin and streptomycin (Invitrogen). Cells were passaged every two days to ensure confluence was kept between 40-70%. Parental C2C12 cells were obtained from ATCC and passages did not exceed 30. Cells were detached for passaging using 0.5% trypsin-EDTA solution (Sigma, T3924). For routine differentiation of parental C2C12, Ctrl and S3^{kd} myoblasts, 90% confluent cultures were washed twice with DMEM

before being cultured in differentiation medium (DMEM, 2% horse serum, 1% pen/strep) for various lengths of time.

Primary muscle stem cell-derived myoblast cultures

Primary muscle stem cell-derived myoblasts (henceforth referred to as MuSC progeny) were obtained from hindlimbs of 8-14 week old male mice (wild type and age-matched *Sdc3*$^{-/-}$) as described previously [51, 63]. Growth medium consisted of F12 + 0.4 mM CaCl2 (F12C), 15% horse serum (HyClone), 1% penicillin/streptomycin, 2 nM recombinant FGF2 (kindly donated by Dr David Fernig, University of Liverpool). MuSC progeny were passaged once, two days after initial isolation and plating, using 40 units/mL of collagenase type I in phosphate buffered saline (PBS). Differentiation medium consisted of F12C, 3% horse serum, 1% penicillin/streptomycin.

Generation of Ctrl and S3^{kd} myoblasts

SDC3 was stably knocked down in C2C12 myoblasts by transfecting cells with a plasmid containing an shRNA sequence that targets SDC3 (Sigma, Mission # TRCN0000071990) to generate the SDC3-depleted (S3^{kd}) cell line, or the empty backbone vector (pLKO-1, Sigma Mission) to generate the control (Ctrl) cell line. C2C12 myoblasts at 80% confluence were transfected using Lipofectamine 2000 then passaged for 3 times in the presence of 2 μg/mL puromycin to select for positively transfected cells. No clonal selection was employed since C2C12 myoblasts are heterogenous. Western blotting was used to confirm knockdown efficiency, which was ≥ 95%.

Western Blotting

Protein extracts were obtained by lysing cells in RIPA buffer (50 mM Tris-HCl, pH 7.4, 1% NP-40, 0.25% sodium-deoxycholate, 150 mM NaCl, and 1 mM EDTA) supplemented with a protease inhibitor cocktail (Complete, Roche) and phosphatase inhibitors (2 mM activated Na_3VO_4, 2 mM NaF and 1x PhosSTOP (Roche)). Soluble proteins were quantified using the Pierce BCA Protein Assay Kit, following the manufacturer's protocol. For detection of all proteins indicated except SDC3, an equal amount of protein sample (between 10-20 μg) was separated by SDS-PAGE and then transferred onto a nitrocellulose membrane (Hybond, GE Healthcare) for two hours at 250 mA on ice. Membranes were blocked with a solution of 5% non-fat milk in Tris Buffered Saline Tween20 (TBST). Primary antibodies (see Table S5) were diluted in either 5% w/v BSA in TBST or 5% milk in TBST, depending on the supplier's recommendation, added to membranes and incubated over night at 4 °C. Membranes were washed in TBST and incubated with a horseradish peroxidase (HRP)-conjugated secondary antibody for one hour at room temperature. After washing with TBST, membranes were visualised

using chemiluminescence (Clarity™ ECL, Biorad) and imaged on an ImageQuant-Las4000 (GE healthcare) gel doc system or Amersham Imager 680. Band intensity was analysed using the 'Analyze Gel' function in ImageJ.

To detect SDC3, cells were lysed as described above and equal amounts of Ctrl and $S3^{kd}$ total protein were precipitated with 2.5x volume of methanol overnight at -20 °C. Precipitates were pelleted by centrifugation at 13,000 x g at 4 °C then washed once with -20 °C acetone and centrifuged again at 4 °C to collect precipitates. After discarding the supernatant, pellets were re-suspended in heparinase buffer (100 mM sodium acetate, 0.1 mM calcium acetate and 1 mM magnesium chloride) and digested with 0.25 mU heparinase III (Ibex) and 0.5 mU chondroitinase-ABC (Sigma-Aldrich) for 2 hours at 37 °C, before addition of another 0.25 mU heparinase III for an additional two hours. Reactions were quenched by addition of 5X SDS-sample buffer and heated to 95 °C for 10 min before 50 µg of protein were loaded onto SDS-PAGE. From this point western blotting were carried out as described above.

Stimulation of Ctrl and $S3^{kd}$ myoblasts with FGF2 or serum

$S3^{kd}$ and Ctrl cells were plated at a density of 45,000 cells per 10 cm plates and cultured for two days. For serum-starvation, cells were washed twice with DMEM and then incubated for 5 hours in DMEM + 2 µg/mL puromycin. After serum-starvation myoblasts were either lysed as described above in the western blotting section or treated with either 10% FBS or 2 nM FGF2 and then lysed at various time points as described in the western blotting section.

Immunostaining, microscopy and quantification

Culture medium was aspirated, and cells fixed with 4% paraformaldehyde (Sigma) in PBS (pH 7.4) solution for 10 minutes at room temperature. Cells were permeabilised with PBS + 0.2% TritonX100 for 10 minutes at room temperature, then washed once with PBS + 0.2% TritonX100 and twice with PBS prior to immunostaining. For detection of myosin heavy chain (MyHC), the primary anti-MyHC antibody (DSHB, MF20 clone) was diluted at 1:150 in PBS + 1% horse serum before being incubated with cells overnight at 4°C. Next, cells were washed as above before a secondary antibody (anti-mouse conjugated to AlexaFluor488) was diluted at 1:500 in PBS + 5% horse serum and incubated with cells for 1 hour at room temperature. A solution of 2 µg/mL DAPI (Life Technologies) in PBS was used to stain DNA. Cells were then washed as above and stored in the dark at 4°C until imaging.

Images were taken using an epifluorescence microscope (EVOS M500, Life Technologies) with the same exposure and gain settings in each experiment.

Quantification of immunostaining was performed by taking a minimum of 20 random images per experiment, with three technical replicates and three biological replicates unless otherwise stated. A bespoke script written for Fiji was used to count DAPI+ nuclei and myotube area as described previously [77]. Differentiation was calculated as the number of nuclei in MyHC positive cells divided by the total number of nuclei x100. Fusion index was calculated as the number nuclei contained in MyHC positives myotubes with at least two nuclei, divided by the total number of nuclei in all MyHC positive cells x100.

Phosphoproteomics sample preparation and LC-MS/MS

Lysates were prepared as previously described [30]. Ctrl and $S3^{kd}$ myoblasts were cultured in growth medium for two days and for each condition four biological replicates were used. Myoblasts were serum-starved for 5 hours in DMEM + 2 µg/mL puromycin then stimulated with FBS for 10 min. Cells were lysed in a mass spectrometry compatible buffer (50 mM ammonium bicarbonate, 0.25% RapiGest™ (Waters, UK), 2 mM NaF, 2 mM Na_3VO_4 and 1x PhosSTOP). Lysates were rotated end-over-end for 30 minutes at 4°C, then sonicated with a Vibracell ultrasonic processor (Sonics, Newtown, USA) on ice for 10 seconds with a tapered microtip. Lysates were then snap-frozen in liquid nitrogen and submitted to the Centre for Proteome Research (CPR), University of Liverpool, for LC-MS/MS analysis. Briefly, 200 µg of protein sample were digested with 0.2 µg/µL trypsin overnight at 37 °C. RapiGest™ was hydrolysed by the addition of trifluoroacetic acid (TFA), for 2 hours at 60 °C, followed by centrifugation at 17,000 x g for 30 minutes at 4 °C. Supernatants were concentrated using a speedvac (Univapo-150 ECH) at a fixed speed of 1,250 rpm, 30 °C for 40 minutes and resuspended in 150 µl of 1% TFA, then desalted on macro spin columns (Harvard Macro Spin Columns). Samples were enriched for phosphopeptides using Titansphere PhosTiO columns (200 µL 5010-21312, Hichrom) prior to being solubilised in 20 µL 1% TFA, and centrifuged at 17,000 *x g* for 15 minutes. 10 µL of supernatant were transferred to total recovery vials for LC-MS/MS analysis. We elected to only run through LC-MS/MS the phosphoproteome-enriched fraction of the cell lysate without running also either the flow through or a separate, unfractionated aliquot. Since signaling proteins are present at low abundance in cells, they are not easily detected by shotgun proteomics without an enrichment step. While the phosphorylated form(s) of these proteins are easier to detect thanks to the TiO_2 enrichment step, their total counterpart is more difficult to detect because of the lack of enrichment and could potentially lead to misleading results. LC-MS/MS was performed at the Centre for Proteome Research, University of Liverpool, UK. Briefly, 4 µL of the phospho-enriched sample were analysed using an Ultimate 3000 RSLC™ nano system (Thermo Scientific, Hemel Hempstead) coupled to a QExactive™

mass spectrometer (Thermo Scientific). The sample was loaded onto the trapping column (Thermo Scientific, PepMap100, C18, 300 µm x 5 mm), for 7 minutes at a flow rate of 9 µL/min with 0.1% TFA and 2% acetonitrile. The sample was resolved on the analytical column (Easy-Spray C18 75 µm x 500 mm 2µm column) using a gradient of 97% buffer A (0.1% formic acid in water) and 3% buffer B (99.9% acetonitrile, 0.1% formic acid) to 60% buffer A and 40% buffer B (all v/v) over 90 minutes at a flow rate of 300 nL/min. The data-dependent program used for data acquisition consisted of a 70,000 resolution full-scan MS scan (automatic gain control (AGC) set to 1 x106 ions with a maximum fill time of 250 ms) and the 10 most abundant peaks were selected for MS/MS using a 35,000 resolution scan (AGC set to 1 x 105 ions with a maximum fill time of 100 ms) with an ion selection window of 2 m/z. To avoid repeated selection of peptides for MS/MS, the program used a 20 second dynamic exclusion window.

Peptide identification and label-free quantification

Peptides were identified using PEAKS Studio 8 searched against the Uniprot *Mus musculus* proteome database (Database version: October 2016). A fixed carbamidomethyl modification for cysteine and variable modifications of oxidation for methionine were specified. A variable modification for phosphorylation of serine, threonine and tyrosine were specified. A precursor mass tolerance of 10 ppm and a fragment ion mass tolerance of 0.05 Da were applied. The results were then filtered to obtain a peptide false discovery rate of 1%. The localisation probability of all putative phosphorylation sites were determined by PEAKS and reported as the Ascore. No filtering of peptides by Ascore was performed.

Chromatogram alignment and label free quantification was performed using Progenesis QI (Version 2.0). Bayesian Markov chain Monte Carlo (MCMC) simulation was performed using the Stan (DOI 10.18637/jss.v076.i01) programming language to fit a Poisson regression model with a log-link for each peptide in each comparison. In cases where a peptide was unobserved in a condition, an informative prior was used to impute a range of potential missing values for that condition. For each condition, a log-linear regression of the peptide abundances against the number of observed data points was used to predict the distribution of abundances of peptides with no observed values. This predicted distribution was then used as an informative prior for the abundance of missing values.

For comparisons #1 - #4, the inferred posterior distributions of the mean log-fold-changes were then used to perform one-sided significance tests to determine the probabilities that the mean fold-change was less than -1.5 or greater than +1.5 for each peptide in each comparison. The complement of the greater of these two probabilities was taken as the quantitative posterior error probability (PEP) for

each peptide in each comparison. For comparison #5, the posterior samples of mean log-fold-change in comparisons #3 and #4 were used to determine the posterior distribution of the difference in log-fold-change between comparison #3 and #4 for each peptide and quantitative PEPs calculated as above. Significant sets of peptides for each of the five comparisons were determined by calculating the largest set where the mean PEP <0.05.

Pathway enrichment analysis

Significantly regulated phosphopeptides and their corresponding Uniprot protein ID, natural log fold change and phosphosite were submitted to Ingenuity Pathway Analysis (IPA, Version 2.3, Qiagen) for canonical pathway enrichment using the phosphoproteome analysis tool. Pathways with an enrichment score of $p < 0.05$ were considered statistically significant. IPA eturns a z-score which gives a prediction of whether pathways detected lead to activation (positive z-score) or deactivation (negative z-score) of that signaling pathway, depending on the proteins and phosphosites that are mapped to that pathway. For Gene Ontology enrichment analysis, DAVID 6.8 [78, 79] was used with significantly regulated phosphoproteins. The background dataset consisted of all the phosphoproteins identified in the phosphoproteomics experiment. Enriched terms with a p-value of less than 0.05 were considered statistically significant.

Co-immunoprecipitation of SDC3 interactors

Immunoprecipitation of SDC3 interactors was performed by fixation of cell lysate as previously described with small modifications [80]. Briefly, C2C12 myoblasts were cultured in normal growth promoting conditions and then gently detached using citric saline (135 mM potassium chloride and 15 mM sodium citrate, no pH adjustment). Cells were pelleted and resuspended to 10^7 cells/mL in 2% paraformaldehyde/PBS solution and incubated for 10 minutes. Cells were pelleted and washed in 0.5 mL ice-cold 1.25 M glycine/PBS solution twice. Cells were then lysed in 1 mL per $1x10^8$ cells with a lysis buffer optimized for immunoprecipitation of heparan sulfate proteoglycans (1 X PBS, 1% Triton X100, 0.1% SDS), for 30 min at 4°C with rotation. After 30 minutes cells were further lysed by passing through a 27G needle 10 times. Lysates were then centrifuged at 17,000 x g at 4 °C for 30 min, soluble extracts were snap-frozen and stored at -80°C.

Protein concentration was determined using the Pierce BCA Protein Assay Kit, following the manufacturer's protocol. 1mg of lysate was diluted in PBS to a volume of 1 mL with the addition of either anti-SDC3 antibody (kindly donated by Dr Alan Rapraeger, University of Wisconsin at Madison, and previously validated by us [26] or normal-rabbit IgG. Antibodies and cell lysate were incubated

overnight at 4 °C with gentle rotation. The next day, immunocomplexes were isolated using protein A agarose beads as directed by the manufacturer's protocol (Pierce, Thermo Fisher). Whilst immunocomplexes were still attached to the beads, glycosaminoglycan chains were removed using heparinase III and chondroitinase ABC as described in the western blotting section. After digestion, immunocomplexes were eluted from the beads by boiling the samples in 2X SDS buffer. Equal volumes of eluted samples were then resolved on an 8% SDS-PAGE and western blotting performed as described above.

Proximity Ligation Assay

Proximity ligation Assay (PLA) was carried out using the DuoLink® kit (Sigma) according to manufacturer instructions. Antibodies to detect SDC3 and INSR-β are specified in Table S6 - Materials and Resources. To quantify the extent to which SDC3 and INSR-β interact, both the number and size of the dots yielded by PLA were measured and an "interaction score" was determined by multiplying number of dots x average dot size for each field of view imaged and quantified under a 20X objective, using an EVOS M5000 microscope, after the background was linearly and homogenously subtracted from the entire image.

Isolation of primary muscle stem cell-derived myoblasts

Hindlimb muscles were dissected and minced before digestion with 400 units/mL collagenase type I in F12C for 1.5 hours at 37 °C with mixing every 15 minutes. Cell pellets were collected and resuspended in primary growth medium before being filtered through a 40 μm cell strainer. Cell pellets were resuspended again and plated onto gelatin-coated dishes under normal culture conditions for 1 hour. Non-adherent cells and growth medium were collected and then re-plated onto new gelatin-coated plates for two hours. For the final plating, non-adherent cells were collected, centrifuged, re-suspended in fresh growth and plated onto fresh gelatin-coated plates for routine culturing.

Stimulation of Ctrl and S3^{kd} and control cells with insulin

For proliferation experiments, Ctrl and S3^{kd} cells were seeded at an equal density in growth medium supplemented with 50 or 100 nM insulin (I0516, Sigma Aldrich) as indicated in figures, or PBS as vehicle control, for 24 hours. During insulin treatment, primary MuSC progeny were maintained without FGF2. After 24 hours, both primary cells and cell lines were fixed and stained with DAPI as described in the immunostaining, microscopy and quantification section.

To measure differentiation and fusion in response to insulin, cells were grown to ~90% confluence before switching them to differentiation medium. All cells were induced to differentiate for three days

in the presence of 100 nM insulin or PBS. Cells were then fixed and stained with DAPI and anti-MyHC antibody as described in the immunostaining, microscopy and quantification section.
To measure the levels of pAKT, AKT, pRPS6, RPS6, ERK1/2 and ERK in proliferating myoblasts, Ctrl and $S3^{kd}$ cells were cultured for two days in growth medium supplemented with 100 nM insulin or PBS. To measure the same protein levels in differentiating cells, Ctrl and $S3^{kd}$ cells were grown to ~90% confluence and then switched to differentiation medium containing either 100 nM insulin or PBS. Cells were differentiated for three days. After the allotted time had passed, cells were lysed and processed for western blotting as described in the relevant section.

Transfection of insulin receptor siRNA in primary myoblasts

For transient knockdown of INSR, primary MuSC progeny were seeded at 8,000 cells/well in 12-multiwell plates in growth medium. For induced differentiation experiments, cells were cultured in growth medium for two days before medium was switched to transfection medium (Opti-MEM + 15% horse serum + 2 nM FGF2), whilst lipofectamine 2000 plus 10 nM INSR siRNAs or scrambled siRNA (sequences in Key Resources Table) were prepared. Lipofectamine 2000 was used as recommended by the manufacturer. Cells were incubated in lipofectamine2000 + siRNAs for five hours and then complexes removed and the culture medium switched to differentiation medium. Cells were left to differentiate for 40 hours before fixation.
For spontaneous differentiation experiments, cells were cultured in growth medium for two days before being switched to transfection medium whilst lipofectamine + siRNAs were being prepared as described above. After five hours the transfection medium was removed and replaced with growth medium minus FGF2 for 48 hours. Cells were fixed and stained as described in the immunostaining, microscopy and quantification section.

Inhibition of AKT in primary MuSC progeny

Primary MuSC progeny were seeded at a density of 7,000 cells/well in 12-multiwell plates in growth medium containing FGF2 and allowed four hours to adhere to the gelatin-coated plates before beginning treatment with an AKT inhibitor (AZD5363, SelleckChem). After culturing in growth medium for 2-3 days, until confluent, FGF2 was removed (by replacing the medium with fresh growth medium that did not contain FGF2) and cultured for an additional two days still in the presence of the AKT inhibitor. A volume of DMSO equal to the volume of AKT inhibitor was added to vehicle control wells. Cells were then fixed and stained with DAPI and anti-MyHC antibody as described above.

Adhesion assay

Ctrl and $S3^{kd}$ myoblasts were detached by trypsin, centrifuged, re-suspended in C2C12 growth medium and counted using a hemacytometer. An equal number of Ctrl and $S3^{kd}$ cells were added to two separate tubes and centrifuged to remove growth medium before being washed twice with either growth medium or serum-free medium (DMEM + 1% penicillin/streptomycin). After the second wash, both sets of cells were centrifuged and re-suspended at 7,000 cells/mL in either DMEM alone or complete growth medium (DMEM + serum). Cells were seeded on laminin (Sigma # L2020, laminin from Engelbreth-Holm-Swarm sarcoma) coated dishes or uncoated dishes and incubated for 1 hour at 37 C, 5% CO_2 before washed once with 1x PBS to remove non-adherent cells, then fixed in 4% PFA for 10 minutes at room temperature and then stained with DAPI to visualise cell nuclei before the number of cells were counted using the bespoke script as described above.

Quantification and statistical analysis

All statistical analysis for biochemistry and immunofluorescence experiments were performed in GraphPad Prism 8. Each experiment contained at least three biological replicates and multiple technical replicates. Data were checked for normal distribution and statistical significance was calculated using the two-tailed Student's t-test or one-way ANOVA followed by Tukey post-test. Data were considered significant if $p < 0.05$. Data were plotted as average ± SEM (standard error of the mean) where error bars are shown.

Supplemental Information Titles

Figure S1. SDC3-depleted cells recapitulated phenotypes observed in *Sdc3*$^{-/-}$ myoblasts, related to Figure 1.

Figure S2. Number of confidently identified peptides, phosphopeptides and phosphosites, related to Figure 2.

Figure S3. SDC3-depleted cells show reduced capacity to adhere to laminin but increased adhesion and FAK signaling on uncoated substrates, related to Figure 2.

Figure S4. Acute insulin stimulation induces robust AKT phosphorylation in both Ctrl and $S3^{kd}$ serum-starved myoblasts, related to Figure 4.

Figure S5. INSR knockdown in wild type myoblasts impairs myoblast fusion without significantly affecting the early stages of differentiation, related to Figure 6.

Figure S6. SDC3 knockdown in myoblasts alters the expression levels of the other three syndecans in differentiating cells but not in proliferating cells. Related to Discussion.

Table S1. Number of of phosphorylated sites identified, related to Figure 2.

Table S2. List of phosphopeptides with significant changes in abundance with both serum stimulation and SDC3 presence/absence, related to Figure 2.

Table S3. List of significantly enriched pathways returned by the IPA analysis of serum stimulated Ctrl cells, related to Figure 3

Table S4. List of significantly enriched pathways returned by the IPA analysis of serum stimulated $S3^{kd}$ cells, related to Figure 3

Table S5. List of tyrosine kinase-related signalling pathways, related to Figure 3.

Table S6. Materials and Resources used, related to all figures.

References

[1] H.C. Olguin, A. Pisconti, Marking the tempo for myogenesis: Pax7 and the regulation of muscle stem cell fate decisions, J Cell Mol Med 16(5) (2012) 1013-25.

[2] N.A. Dumont, Y.X. Wang, M.A. Rudnicki, Intrinsic and extrinsic mechanisms regulating satellite cell function, Development 142(9) (2015) 1572-81.

[3] O. Mashinchian, A. Pisconti, E. Le Moal, C.F. Bentzinger, The Muscle Stem Cell Niche in Health and Disease, Curr Top Dev Biol 126 (2018) 23-65.

[4] E. Brandan, J. Gutierrez, Role of skeletal muscle proteoglycans during myogenesis, Matrix Biol 32(6) (2013) 289-97.

[5] W.M. Han, Y.C. Jang, A.J. Garcia, Engineered matrices for skeletal muscle satellite cell engraftment and function, Matrix Biol 60-61 (2017) 96-109.

[6] R. Droguett, C. Cabello-Verrugio, C. Riquelme, E. Brandan, Extracellular proteoglycans modify TGF-beta bio-availability attenuating its signaling during skeletal muscle differentiation, Matrix Biol 25(6) (2006) 332-41.

[7] Z. Xu, N. Ichikawa, K. Kosaki, Y. Yamada, T. Sasaki, L.Y. Sakai, H. Kurosawa, N. Hattori, E. Arikawa-Hirasawa, Perlecan deficiency causes muscle hypertrophy, a decrease in myostatin expression, and changes in muscle fiber composition, Matrix Biol 29(6) (2010) 461-70.

[8] D.L. Rebolledo, D. Gonzalez, J. Faundez-Contreras, O. Contreras, C.P. Vio, J.E. Murphy-Ullrich, K.E. Lipson, E. Brandan, Denervation-induced skeletal muscle fibrosis is mediated by CTGF/CCN2 independently of TGF-beta, Matrix Biol 82 (2019) 20-37.

[9] R. Valle-Tenney, D.L. Rebolledo, K.E. Lipson, E. Brandan, Role of hypoxia in skeletal muscle fibrosis: Synergism between hypoxia and TGF-beta signaling upregulates CCN2/CTGF expression specifically in muscle fibers, Matrix Biol 87 (2020) 48-65.

[10] A. Pisconti, J.D. Bernet, B.B. Olwin, Syndecans in skeletal muscle development, regeneration and homeostasis., Muscles, ligaments and tendons journal 2(1) (2012) 1-9.

[11] M.C. Fisher, Y. Li, M.R. Seghatoleslami, C.N. Dealy, R.A. Kosher, Heparan sulfate proteoglycans including syndecan-3 modulate BMP activity during limb cartilage differentiation, Matrix Biol 25(1) (2006) 27-39.

[12] A. Woods, E.S. Oh, J.R. Couchman, Syndecan proteoglycans and cell adhesion, Matrix Biol 17(7) (1998) 477-83.

[13] F.K. Jones, A. Stefan, A.G. Kay, M. Hyland, R. Morgan, N.R. Forsyth, A. Pisconti, O. Kehoe, Syndecan-3 regulates MSC adhesion, ERK and AKT signalling in vitro and its deletion enhances MSC efficacy in a model of inflammatory arthritis in vivo, Sci Rep 10(1) (2020) 20487.

[14] S.B. Ronning, C.R. Carlson, J.M. Aronsen, A. Pisconti, V. Host, M. Lunde, K.H. Liland, I. Sjaastad, S.O. Kolset, G. Christensen, M.E. Pedersen, Syndecan-4(-/-) Mice Have Smaller Muscle Fibers, Increased Akt/mTOR/S6K1 and Notch/HES-1 Pathways, and Alterations in Extracellular Matrix Components, Front Cell Dev Biol 8 (2020) 730.

[15] J.R. Whiteford, V. Behrends, H. Kirby, M. Kusche-Gullberg, T. Muramatsu, J.R. Couchman, Syndecans promote integrin-mediated adhesion of mesenchymal cells in two distinct pathways, Exp Cell Res 313(18) (2007) 3902-13.

[16] J.R. Couchman, Syndecans: proteoglycan regulators of cell-surface microdomains?, Nat Rev Mol Cell Biol 4(12) (2003) 926-37.

[17] A.N. Alexopoulou, H.A. Multhaupt, J.R. Couchman, Syndecans in wound healing, inflammation and vascular biology, Int J Biochem Cell Biol 39(3) (2007) 505-28.

[18] A.J. De Micheli, E.J. Laurilliard, C.L. Heinke, H. Ravichandran, P. Fraczek, S. Soueid-Baumgarten, I. De Vlaminck, O. Elemento, B.D. Cosgrove, Single-Cell Analysis of the Muscle

Stem Cell Hierarchy Identifies Heterotypic Communication Signals Involved in Skeletal Muscle Regeneration, Cell Rep 30(10) (2020) 3583-3595 e5.

[19] D.D. Cornelison, M.S. Filla, H.M. Stanley, A.C. Rapraeger, B.B. Olwin, Syndecan-3 and syndecan-4 specifically mark skeletal muscle satellite cells and are implicated in satellite cell maintenance and muscle regeneration, Dev Biol 239(1) (2001) 79-94.

[20] H. Olguin, E. Brandan, Expression and localization of proteoglycans during limb myogenic activation, Dev Dyn 221(1) (2001) 106-15.

[21] X. Liu, D.C. McFarland, K.E. Nestor, S.G. Velleman, Developmental regulated expression of syndecan-1 and glypican in pectoralis major muscle in turkeys with different growth rates, Dev Growth Differ 46(1) (2004) 37-51.

[22] S.G. Velleman, Y. Song, Development and Growth of the Avian Pectoralis Major (Breast) Muscle: Function of Syndecan-4 and Glypican-1 in Adult Myoblast Proliferation and Differentiation, Front Physiol 8 (2017) 577.

[23] J.C. Casar, C. Cabello-Verrugio, H. Olguin, R. Aldunate, N.C. Inestrosa, E. Brandan, Heparan sulfate proteoglycans are increased during skeletal muscle regeneration: requirement of syndecan-3 for successful fiber formation, J Cell Sci 117(Pt 1) (2004) 73-84.

[24] L. Fuentealba, D.J. Carey, E. Brandan, Antisense inhibition of syndecan-3 expression during skeletal muscle differentiation accelerates myogenesis through a basic fibroblast growth factor-dependent mechanism, J Biol Chem 274(53) (1999) 37876-84.

[25] A. Pisconti, G.B. Banks, F. Babaeijandaghi, N.D. Betta, F.M. Rossi, J.S. Chamberlain, B.B. Olwin, Loss of niche-satellite cell interactions in syndecan-3 null mice alters muscle progenitor cell homeostasis improving muscle regeneration, Skelet Muscle 6 (2016) 34.

[26] A. Pisconti, D.D. Cornelison, H.C. Olguin, T.L. Antwine, B.B. Olwin, Syndecan-3 and Notch cooperate in regulating adult myogenesis, J Cell Biol 190(3) (2010) 427-41.

[27] J. Shin, D.C. McFarland, S.G. Velleman, Migration of turkey muscle satellite cells is enhanced by the syndecan-4 cytoplasmic domain through the activation of RhoA, Mol Cell Biochem 375(1-2) (2013) 115-30.

[28] D.D. Cornelison, S.A. Wilcox-Adelman, P.F. Goetinck, H. Rauvala, A.C. Rapraeger, B.B. Olwin, Essential and separable roles for Syndecan-3 and Syndecan-4 in skeletal muscle development and regeneration, Genes Dev 18(18) (2004) 2231-6.

[29] C.F. Bentzinger, Y.X. Wang, J. von Maltzahn, V.D. Soleimani, H. Yin, M.A. Rudnicki, Fibronectin regulates Wnt7a signaling and satellite cell expansion., Cell Stem Cell 12(1) (2013) 75-87.

[30] F.K. Jones, G.E. Hardman, S. Ferries, C.E. Eyers, A. Pisconti, Myoblast Phosphoproteomics as a Tool to Investigate Global Signaling Events During Myogenesis, Methods Mol Biol 1889 (2019) 301-317.

[31] L.S. Harrington, G.M. Findlay, R.F. Lamb, Restraining PI3K: mTOR signalling goes back to the membrane, Trends Biochem Sci 30(1) (2005) 35-42.

[32] O.J. Shah, T. Hunter, Turnover of the active fraction of IRS1 involves raptor-mTOR- and S6K1-dependent serine phosphorylation in cell culture models of tuberous sclerosis, Mol Cell Biol 26(17) (2006) 6425-34.

[33] T. Haruta, T. Uno, J. Kawahara, A. Takano, K. Egawa, P.M. Sharma, J.M. Olefsky, M. Kobayashi, A rapamycin-sensitive pathway down-regulates insulin signaling via phosphorylation and proteasomal degradation of insulin receptor substrate-1, Mol Endocrinol 14(6) (2000) 783-94.

[34] A.D. Sharrocks, Cell cycle: sustained ERK signalling represses the inhibitors, Curr Biol 16(14) (2006) R540-2.

[35] Y.D. Shaul, R. Seger, The MEK/ERK cascade: from signaling specificity to diverse functions, Biochim Biophys Acta 1773(8) (2007) 1213-26.

[36] H. Lavoie, J. Gagnon, M. Therrien, ERK signalling: a master regulator of cell behaviour, life and fate, Nat Rev Mol Cell Biol 21(10) (2020) 607-632.

[37] S. Li, P. Mattar, R. Dixit, S.O. Lawn, G. Wilkinson, C. Kinch, D. Eisenstat, D.M. Kurrasch, J.A. Chan, C. Schuurmans, RAS/ERK signaling controls proneural genetic programs in cortical development and gliomagenesis, J Neurosci 34(6) (2014) 2169-90.

[38] J.H. Rhim, X. Luo, D. Gao, X. Xu, T. Zhou, F. Li, P. Wang, S.T. Wong, X. Xia, Cell type-dependent Erk-Akt pathway crosstalk regulates the proliferation of fetal neural progenitor cells, Sci Rep 6 (2016) 26547.

[39] L. Xing, R.S. Larsen, G.R. Bjorklund, X. Li, Y. Wu, B.D. Philpot, W.D. Snider, J.M. Newbern, Layer specific and general requirements for ERK/MAPK signaling in the developing neocortex, Elife 5 (2016).

[40] J. Boucher, A. Kleinridders, C.R. Kahn, Insulin receptor signaling in normal and insulin-resistant states, Cold Spring Harb Perspect Biol 6(1) (2014).

[41] J.B. Hwang, S.C. Frost, Effect of alternative glycosylation on insulin receptor processing, J Biol Chem 274(32) (1999) 22813-20.

[42] K. Machackova, M. Chrudinova, J. Radosavljevic, P. Potalitsyn, K. Krizkova, M. Fabry, I. Selicharova, M. Collinsova, A.M. Brzozowski, L. Zakova, J. Jiracek, Converting Insulin-like Growth Factors 1 and 2 into High-Affinity Ligands for Insulin Receptor Isoform A by the Introduction of an Evolutionarily Divergent Mutation, Biochemistry 57(16) (2018) 2373-2382.

[43] F. Frasca, G. Pandini, P. Scalia, L. Sciacca, R. Mineo, A. Costantino, I.D. Goldfine, A. Belfiore, R. Vigneri, Insulin receptor isoform A, a newly recognized, high-affinity insulin-like growth factor II receptor in fetal and cancer cells, Mol Cell Biol 19(5) (1999) 3278-88.

[44] Y. Yamaguchi, J.S. Flier, H. Benecke, B.J. Ransil, D.E. Moller, Ligand-binding properties of the two isoforms of the human insulin receptor, Endocrinology 132(3) (1993) 1132-8.

[45] S. Benyoucef, K.H. Surinya, D. Hadaschik, K. Siddle, Characterization of insulin/IGF hybrid receptors: contributions of the insulin receptor L2 and Fn1 domains and the alternatively spliced exon 11 sequence to ligand binding and receptor activation, Biochem J 403(3) (2007) 603-13.

[46] A. Denley, E.R. Bonython, G.W. Booker, L.J. Cosgrove, B.E. Forbes, C.W. Ward, J.C. Wallace, Structural determinants for high-affinity binding of insulin-like growth factor II to insulin receptor (IR)-A, the exon 11 minus isoform of the IR, Mol Endocrinol 18(10) (2004) 2502-12.

[47] R. Conejo, A.M. Valverde, M. Benito, M. Lorenzo, Insulin produces myogenesis in C2C12 myoblasts by induction of NF-kappaB and downregulation of AP-1 activities, J Cell Physiol 186(1) (2001) 82-94.

[48] K. Grabiec, M. Gajewska, M. Milewska, M. Blaszczyk, K. Grzelkowska-Kowalczyk, The influence of high glucose and high insulin on mechanisms controlling cell cycle progression and arrest in mouse C2C12 myoblasts: the comparison with IGF-I effect, J Endocrinol Invest 37(3) (2014) 233-45.

[49] K. Grzelkowska-Kowalczyk, W. Wieteska-Skrzeczynska, K. Grabiec, J. Tokarska, High glucose-mediated alterations of mechanisms important in myogenesis of mouse C2C12 myoblasts, Cell Biol Int 37(1) (2013) 29-35.

[50] J.L. Mandel, M.L. Pearson, Insulin stimulates myogenesis in a rat myoblast line, Nature 251(5476) (1974) 618-20.

[51] V. Flamini, R.S. Ghadiali, P. Antczak, A. Rothwell, J.E. Turnbull, A. Pisconti, The Satellite Cell Niche Regulates the Balance between Myoblast Differentiation and Self-Renewal via p53, Stem Cell Reports 10(3) (2018) 970-983.

[52] N.C. Jones, Y.V. Fedorov, R.S. Rosenthal, B.B. Olwin, ERK1/2 is required for myoblast proliferation but is dispensable for muscle gene expression and cell fusion, J Cell Physiol 186(1) (2001) 104-15.

[53] L.L. Arnold, A. Cecchini, D.A. Stark, J. Ihnat, R.N. Craigg, A. Carter, S. Zino, D. Cornelison, EphA7 promotes myogenic differentiation via cell-cell contact, Elife 9 (2020).

[54] G. Cossu, R. Kelly, S. Di Donna, E. Vivarelli, M. Buckingham, Myoblast differentiation during mammalian somitogenesis is dependent upon a community effect, Proc Natl Acad Sci U S A 92(6) (1995) 2254-8.

[55] P. Zhang, C. Wong, D. Liu, M. Finegold, J.W. Harper, S.J. Elledge, p21(CIP1) and p57(KIP2) control muscle differentiation at the myogenin step, Genes Dev 13(2) (1999) 213-24.

[56] O. Halevy, B.G. Novitch, D.B. Spicer, S.X. Skapek, J. Rhee, G.J. Hannon, D. Beach, A.B. Lassar, Correlation of terminal cell cycle arrest of skeletal muscle with induction of p21 by MyoD, Science 267(5200) (1995) 1018-21.

[57] S. Ruijtenberg, S. van den Heuvel, Coordinating cell proliferation and differentiation: Antagonism between cell cycle regulators and cell type-specific gene expression, Cell Cycle 15(2) (2016) 196-212.

[58] M.F. Buas, T. Kadesch, Regulation of skeletal myogenesis by Notch, Exp Cell Res 316(18) (2010) 3028-33.

[59] H.C. Olguín, B.B. Olwin, Pax-7 up-regulation inhibits myogenesis and cell cycle progression in satellite cells: a potential mechanism for self-renewal., Dev Biol 275(2) (2004) 375-388.

[60] H.C. Olguin, Z. Yang, S.J. Tapscott, B.B. Olwin, Reciprocal inhibition between Pax7 and muscle regulatory factors modulates myogenic cell fate determination, The Journal of cell biology 177(5) (2007) 769-779.

[61] A.J. Goel, M.K. Rieder, H.H. Arnold, G.L. Radice, R.S. Krauss, Niche Cadherins Control the Quiescence-to-Activation Transition in Muscle Stem Cells, Cell Rep 21(8) (2017) 2236-2250.

[62] J.D. Knight, R. Kothary, The myogenic kinome: protein kinases critical to mammalian skeletal myogenesis, Skelet Muscle 1 (2011) 29.

[63] R.S. Ghadiali, S.E. Guimond, J.E. Turnbull, A. Pisconti, Dynamic changes in heparan sulfate during muscle differentiation and ageing regulate myoblast cell fate and FGF2 signalling., Matrix Biol (2016).

[64] J.G.t. Taylor, A.T. Cheuk, P.S. Tsang, J.Y. Chung, Y.K. Song, K. Desai, Y. Yu, Q.R. Chen, K. Shah, V. Youngblood, J. Fang, S.Y. Kim, C. Yeung, L.J. Helman, A. Mendoza, V. Ngo, L.M. Staudt, J.S. Wei, C. Khanna, D. Catchpoole, S.J. Qualman, S.M. Hewitt, G. Merlino, S.J. Chanock, J. Khan, Identification of FGFR4-activating mutations in human rhabdomyosarcomas that promote metastasis in xenotransplanted models, J Clin Invest 119(11) (2009) 3395-407.

[65] H. Rees, D. Williamson, A. Papanastasiou, N. Jina, S. Nabarro, J. Shipley, J. Anderson, The MET receptor tyrosine kinase contributes to invasive tumour growth in rhabdomyosarcomas, Growth Factors 24(3) (2006) 197-208.

[66] K. Vuori, E. Ruoslahti, Association of insulin receptor substrate-1 with integrins, Science 266(5190) (1994) 1576-8.

[67] S. El Annabi, N. Gautier, V. Baron, Focal adhesion kinase and Src mediate integrin regulation of insulin receptor phosphorylation, FEBS Lett 507(3) (2001) 247-52.

[68] D.M. Beauvais, A.C. Rapraeger, Syndecan-1-mediated cell spreading requires signaling by alphavbeta3 integrins in human breast carcinoma cells, Exp Cell Res 286(2) (2003) 219-32.

[69] Y. Tajiri, T. Kato, H. Nakayama, K. Yamada, Reduction of skeletal muscle, especially in lower limbs, in Japanese type 2 diabetic patients with insulin resistance and cardiovascular risk factors, Metab Syndr Relat Disord 8(2) (2010) 137-42.

[70] D.M. D'Souza, D. Al-Sajee, T.J. Hawke, Diabetic myopathy: impact of diabetes mellitus on skeletal muscle progenitor cells, Front Physiol 4 (2013) 379.

[71] J.M. Peterson, R.W. Bryner, S.E. Alway, Satellite cell proliferation is reduced in muscles of obese Zucker rats but restored with loading, Am J Physiol Cell Physiol 295(2) (2008) C521-8.

[72] A.D. Strader, O. Reizes, S.C. Woods, S.C. Benoit, R.J. Seeley, Mice lacking the syndecan-3 gene are resistant to diet-induced obesity, J Clin Invest 114(9) (2004) 1354-60.

[73] B.C. Chang, L.C. Hwang, W.H. Huang, Positive Association of Metabolic Syndrome with a Single Nucleotide Polymorphism of Syndecan-3 (rs2282440) in the Taiwanese Population, Int J Endocrinol 2018 (2018) 9282598.

[74] K.L. Kua, S. Hu, C. Wang, J. Yao, D. Dang, A.B. Sawatzke, J.L. Segar, K. Wang, A.W. Norris, Fetal hyperglycemia acutely induces persistent insulin resistance in skeletal muscle, J Endocrinol 242(1) (2019) M1-M15.

[75] Y. Perez-Riverol, A. Csordas, J. Bai, M. Bernal-Llinares, S. Hewapathirana, D.J. Kundu, A. Inuganti, J. Griss, G. Mayer, M. Eisenacher, E. Perez, J. Uszkoreit, J. Pfeuffer, T. Sachsenberg, S. Yilmaz, S. Tiwary, J. Cox, E. Audain, M. Walzer, A.F. Jarnuczak, T. Ternent, A. Brazma, J.A. Vizcaino, The PRIDE database and related tools and resources in 2019: improving support for quantification data, Nucleic Acids Res 47(D1) (2019) D442-D450.

[76] O. Reizes, J. Lincecum, Z. Wang, O. Goldberger, L. Huang, M. Kaksonen, R. Ahima, M.T. Hinkes, G.S. Barsh, H. Rauvala, M. Bernfield, Transgenic expression of syndecan-1 uncovers a physiological control of feeding behavior by syndecan-3, Cell 106(1) (2001) 105-116.

[77] N. Arecco, C.J. Clarke, F.K. Jones, D.M. Simpson, D. Mason, R.J. Beynon, A. Pisconti, Elastase levels and activity are increased in dystrophic muscle and impair myoblast cell survival, proliferation and differentiation., Scientific reports 6 (2016) 24708.

[78] W. Huang da, B.T. Sherman, R.A. Lempicki, Systematic and integrative analysis of large gene lists using DAVID bioinformatics resources, Nat Protoc 4(1) (2009) 44-57.

[79] W. Huang da, B.T. Sherman, R.A. Lempicki, Bioinformatics enrichment tools: paths toward the comprehensive functional analysis of large gene lists, Nucleic acids research 37(1) (2009) 1-13.

[80] C. Klockenbusch, J. Kast, Optimization of formaldehyde cross-linking for protein interaction analysis of non-tagged integrin beta1, J Biomed Biotechnol 2010 (2010) 927585.